Paper accepted for publication in Langmuir
doi: 10.1021/acs.langmuir.8b02771

Multilayer formation in self-shaping emulsion droplets

Diana Cholakova,[1] Nikolai Denkov*,[1] Slavka Tcholakova,[1] Zhulieta Valkova,[1] Stoyan K. Smoukov[2]

[1]*Department of Chemical and Pharmaceutical Engineering*
Faculty of Chemistry and Pharmacy, Sofia University,
1 James Bourchier Avenue, 1164 Sofia, Bulgaria
[2] *Active and Intelligent Materials Lab, School of Engineering and Materials Science, Queen Mary University of London, Mile End Road, London E14NS, UK*

*Corresponding author:
Prof. Nikolai Denkov
Department of Chemical and Pharmaceutical Engineering
Sofia University
1 James Bourchier Ave.,
Sofia 1164
Bulgaria
E-mail: nd@lcpe.uni-sofia.bg
Tel: +359 2 8161639
Fax: +359 2 9625643

ABSTRACT

In several recent studies we showed that micrometer sized oil-in-water emulsion droplets from alkanes, alkenes, alcohols, triglycerides or mixtures of these components can spontaneously "self-shape" upon cooling into various regular shapes, such as regular polyhedrons, platelets, rods and fibers (Denkov et al., *Nature* 2015, *528*, 392; Cholakova et al., *Adv. Colloid Interface Sci.* 2016, *235*, 90). These drop-shape transformations were explained by assuming that intermediate plastic rotator phase, composed of ordered multilayers of oily molecules, is formed beneath the drop surface around the oil freezing temperature. An alternative explanation was proposed by Guttman et al. (*PNAS* 2016, *113*, 493; *Langmuir* 2017, *33*, 1305) which is based on the assumption that the oil-water interfacial tension decreases to very low values upon emulsion cooling. Here we present new results, obtained by differential scanning calorimetry (DSC), which quantify the enthalpy effects accompanying the drop-shape transformations. Using optical microscopy we related the peaks in the DSC thermograms to the specific changes in the drop shape. Furthermore, from the enthalpies measured by DSC we determined the fraction of the intermediate phase involved in the processes of drop deformation. The obtained results support the explanation that the drop-shape transformations are intimately related to formation of ordered multilayers of alkane molecules with a thickness varying between several and dozens of layers of alkane molecules, depending on the specific system. The new results provide the basis for a rational approach to the mechanistic explanation and to the fine control of this fascinating and industrially relevant phenomenon.

INTRODUCTION

Recently we showed[1-4] that micrometer in size emulsion droplets, stabilized by long-chain surfactants, can spontaneously change their shape several times upon cooling, before the ultimate drop freezing (solidification). A general drop-shape evolution sequence was observed in which the droplets first transform from spheres into fluid polyhedrons that gradually flatten and form hexagonal platelets. These hexagonal platelets can further evolve into either tetrangular platelets which ultimately transform into rods and/or thin fibers, or into triangular platelets from the acute angles of which protrusions may grow, see Supporting Information **Figure S1**. This phenomenon was observed with a variety of non-polar (oily) substances, including *n*-alkanes, 1-alkenes, 1-alcohols, triglycerides and their mixtures.[1-4] Furthermore, we observed this phenomenon with substances which do not create self-shaping drops (when used as single components in the oily drops) after mixing them with a moderate amount, above ca. 15 vol. %, of another substance which produce self-shaping droplets upon cooling.[4] The evolution sequence, shown in **Figure S1**, is common for all tested emulsions. However, different stages of this sequence could be reached in the moment of drop freezing, depending mainly on the specific surfactant-oil combination, the initial drop size and the rate of emulsion cooling. Also, for small initial droplets with diameter approaching that of the final rods and fibers, the evolution processes are kinetically faster (under otherwise equivalent conditions) and the process of drop flattening may merge with the elongation to rods and fibers. Depending on the specific oil-surfactant couple used, the spontaneous transformations were observed to start at a temperature which is a few degrees above, just around, or a few degrees below the bulk melting temperature of the oily phase.[2]

This "self-shaping" phenomenon is of interest for several reasons. On one side, it provides a new, highly-efficient method for producing micrometer-sized particles with complex regular shapes. These particles could be polymerized, thus producing regular in shape polymeric microparticles.[5] On the other side, these systems serve as a new type of versatile toolbox for studying minimal in composition systems which show complex morphogenesis transformations, thus providing insight into the mechanisms generating structure and shape in nature.[2,6] In addition, new low-temperature method for self-emulsification[7-8] was discovered for some of these systems, which is mechanistically based on the drop self-shaping phenomenon and is applicable to temperature sensitive compounds such as some medical drugs, food supplements and flavors.

The "self-shaping" phenomenon is far from trivial, because it involves a spontaneous increase of the drop surface area with related increase of the system interfacial energy. The drop deformation occurs against the capillary pressure which acts as to preserve the spherical shape of the drops. To explain this non-trivial phenomenon, in our original studies[1-3] we proposed a mechanism which includes the formation of *molecular multilayers* of plastic rotator phase,[9-12] templated by the frozen surfactant adsorption layer, see Supporting Information **Figure S1**. Indeed, such plastic rotator phases were detected in cooled alkane droplets by X-ray diffraction in earlier studies.[13-15] In our mechanism, the formed multilayer of plastic rotator phase counteracts the finite interfacial tension of the drop surface (of the order of several to 10 mN/m) due to its significant mechanical strength (viz. to its inherent plasto-elastic nature). We estimated theoretically the thickness of the rotator phase by making a balance between the bending energy of a plastic surface sheet and the surface energy of the deforming drops.[1] From this estimate we calculated that the thickness of the rotator phase should be of the order of 15-300 nm.[1-2,16]

An alternative explanation of the same phenomenon was proposed independently by Guttman et al.[17-19] These authors assumed that the interfacial tension of the cooled emulsion drops approaches zero and, therefore, the observed drop shape transformations could be effectuated by the mechanical strength of the *surfactant adsorption monolayer*, including intercalated alkane molecules,[18] after its freezing on the drop surface.

However, in our previous study[3] we measured the temperature dependence of the interfacial tensions of several systems undergoing such drop-shape transitions and our results showed unambiguously that drop self-shaping is not related to ultralow oil−water interfacial tension, because the drop-shape transformations typically start at temperatures at which the interfacial tension is in the range between 4 and 8 mN/m for all systems studied by us.

The two alternative mechanisms inevitably focus on different key factors when analyzing the fine details in the mechanism and the main factors for control of the self-shaping and self-emulsification phenomena. The mechanism by Denkov et al. focuses on the conditions for formation of rotator phases in the oily drops, whereas the mechanism by Guttman et al. focuses on the conditions for obtaining very low oil-water interfacial tension. Thus, without having clarity about the underlying mechanism, it is very difficult to approach in a rational way the key questions at the current stage of understanding - how to control and to optimize the phenomena of drop self-shaping and self-emulsification for specific systems and applications.

To clarify the detailed mechanism of the observed drop-shape transformations and to determine the thickness of the surface molecular layers which are directly involved in these transformations, in the current study we apply differential scanning calorimetry (DSC) to cooled

emulsions. DSC is a powerful and very sensitive technique for quantification of the enthalpies of phase transitions.[20] This method is widely used for characterization and analysis of the phase transitions in polymer, ceramic, organic and inorganic, food and pharmaceutical systems, and even in biological organisms.[20-32] DSC has been used also to study the phase transformations in emulsions.[33-40]

The direct characteristics which can be obtained from a typical DSC experiment on emulsions, consisting of one cooling and subsequent heating cycle, are the temperatures and enthalpies of freezing and melting transitions, the emulsion type and the fraction of the dispersed phase/medium which undergoes phase transitions.[33-35] As mentioned above, plastic rotator phases were first detected by X-ray diffraction in cooled emulsions containing alkane droplets, in studies which sometimes involved DSC measurements as well.[13-15] In these studies, the droplets were not observed by optical microscopy and, therefore, it has remained unclear whether drop-shape transformations occurred. DSC studies of similar emulsions were performed also by Gülseren and Coupland.[40] These authors studied emulsions containing much smaller droplets, with sub-micrometer diameter, and alkanes with longer chain-length (compared to the emulsions studied by us) for which the existence of rotator phases upon cooling had been detected earlier.[41] Therefore, these previous papers do not provide direct answers to the research questions which have motivated our current study.

Here we combine for the first time systematic DSC measurements on emulsions containing "self-shaping" droplets with observations of the drop transformations by optical microscopy. Thus we are able to determine the fraction of the drop material undergoing phase transition in the temperature range in which the drop-shape transformations occur. The obtained results show that the drop-shape transformations are caused by formation of ordered multilayers of alkane molecules, with a thickness depending strongly on the specific alkane-surfactant combination.

EXPERIMENTAL SECTION

MATERIALS

As dispersed phase we use two linear *n*-alkanes – hexadecane ($C_{16}H_{34}$) and dodecane ($C_{12}H_{26}$) both with purity of 99%, purchased from Sigma-Aldrich. Detailed information for the physical properties of these alkanes is presented in Supporting information **Table S1**. Hexadecane was purified from possible surface-active contaminations by passing it through a glass column filled with Florisil adsorbent. Very similar results were obtained with purified and non-purified hexadecanes. Therefore, the dodecane was used as received.

For emulsion stabilization we used the following series of water-soluble nonionic surfactants (in parentheses – their trade name): the polyoxyethylene alkyl ethers $C_{16}EO_{20}$ (Brij 58), $C_{16}EO_{10}$ (Brij C10) and $C_{16\text{-}18}EO_{50}$ (Lutensol AT50), and the polyoxyethylene sorbitan monoalkylates $C_{12}SorbEO_{23}$ (Tween 20) and $C_{16}SorbEO_{20}$ (Tween 40). All surfactants, except Lutensol AT50 (product of BASF), were purchased from Sigma-Aldrich and were used without further purification. Information for the surfactant properties is presented in Supporting information **Table S2**.

All aqueous solutions were prepared with deionized water with resistivity > 18 MΩ·cm, purified by Elix 3 module (Millipore). The surfactant concentration was 1.5 wt % in all systems studied, emulsions and surfactant solutions, except for Brij C10 (0.75 wt %), always being well above the critical micellar concentration (CMC) of these surfactants.

METHODS

Emulsion preparation.

All emulsions were prepared by membrane emulsification in which drops with relatively narrow size-distribution are generated.[42-45] The polydispersity index, defined as $\sigma = d_{V84}/d_{V50}$,[46] was 1.14 ± 0.04 for all studied emulsions. We used a laboratory Microkit membrane emulsification module from Shirasu Porous Glass Technology (SPG, Miyazaki, Japan), working with tubular glass membranes of outer diameter 10 mm and working area of approx. 3 cm^2. The non-polar (oily) phase was emulsified by passing it through the membrane pores under pressure, into the continuous phase (aqueous surfactant solution). Membranes with mean pore diameter of 1 μm, 2 μm, 3 μm or 10 μm were used to prepare emulsions with different mean drop diameters. Typically, drops with diameter around 3 times bigger than the pore diameter are produced by this method.[44]

DSC experiments

All DSC experiments were performed on Discovery DSC 250 apparatus (TA Instruments, USA). A sample of the studied emulsion (oil weight fraction, Φ, between 0.3 and 10 %) was weighted and placed into a DSC pan (Tzero pan, TA Instruments). Hermetic lid and Tzero sample press (Tzero hermetic lid, TA Instruments) were used to seal the DSC pan before measurements. The samples were cooled and heated at a fixed rate. Based on the results from preliminary experiments, this rate was fixed at 0.5 °C/min in all measurements used to determine the thickness of the multilayers. The reason to choose this rate is that the enthalpy peaks are sufficiently large while the cooling is still sufficiently slow to allow extensive drop shape evolution before the final drop crystallization. The DSC curves upon both cooling and heating

were recorded. We performed one cooling and one heating cycle only, because of the possible drop-drop coalescence during the heating process. For all studied systems, at least three independent samples were tested (usually, between 5 and 10) to obtain sufficient experimental data for statistical analysis and for checking the reproducibility of the final results.

The integration of the DSC curves was performed using the built-in functions of the TRIOS data analysis software (TA Instruments). No baseline subtraction or any other data manipulation was made to determine the peak areas in the thermograms. The horizontal dashed lines drawn in the thermograms, as shown in the figures throughout the paper, are used as guides to the eye only. To allow direct comparison between the various thermograms, in all figures the thermograms are shifted in vertical direction so that the baseline value is set at zero and the y-axis is rescaled, so that the total peaks' area corresponds to the total bulk melting enthalpy of the oil contained in the emulsion sample (as determined upon heating). All these changes affect the visual representation of the DSC data in the figures only – they do not affect in any way the peak areas ratios determined by the built-in TRIOS data analysis software of TA Instruments.

Optical observation in a capillary.

For microscope observations[1-4] of the self-shaping drops, a specimen of the studied emulsion was placed in a rectangular glass capillary with length of 50 mm, width of 1 mm and height of 0.1 mm. This capillary was enclosed within a custom-made metal cooling chamber, with optical windows for microscope observation, see Supporting information **Figure S2**. The chamber temperature was controlled by cryo-thermostat (JULABO CF30, Cryo-Compact Circulator). The temperature in the sample during the experiment was measured using a calibrated thermo-couple probe with an accuracy of ± 0.2°C. The thermo-probe was inserted in one of the orifices of the aluminium thermostating chamber and mounted at a position, where a capillary with the emulsion sample would be normally placed for microscope observations. In the neighbouring orifices the actual capillaries with the emulsion samples were placed. The correct measurement of the temperature was ensured by calibrating the thermo-couple with a precise mercury thermometer in the range of temperatures measured. After freezing the oily drops, we heated them up until the melting process was observed. We always observe the melting process at temperatures very close, within ± 0.2°C, to the reported melting temperature of the bulk oil, T_m, see Supporting information **Table S1**. The rate of emulsion cooling during these optical observations was the same as in the DSC experiments with the same emulsion, thus allowing comparison of the obtained DSC thermograms with the drop shape transformations.

All optical observations were performed with AxioImager.M2m microscope (Zeiss, Germany). We used transmitted, cross-polarized white light, with included λ-compensator plate, situated after the sample and before the analyser, at 45° with respect to both the analyser and the polarizer. Under these conditions the liquid background and the fluid objects have typical magenta color, whereas the frozen birefringent areas appear brighter and may have intense colors.[47-48] We used transmitted light when taking images for determination of the drop size distribution. Long-focus objectives ×20, ×50 and ×100 were used.

We note that although the oil weight fraction in the studied emulsions is relatively low, the emulsion droplets are able cream upwards in the capillary, under the action of buoyancy. Therefore, the microscopy images presented throughout the paper show a relatively dense monolayer of droplets that creamed from the entire emulsion layer, thus forming a layer with an increased local concentration of the drops.

Optical observation in a DSC pan

To check for the actual behaviour of the studied emulsion droplets during cooling and heating in the DSC experiments, we performed additional optical observations of emulsion samples, placed in a DSC pan. These experiments were performed as follows: two open DSC pans, containing equivalent emulsion samples, were placed in a metal cooling chamber, connected to a thermostat. One of the pans was used for optical observations in white reflected light, while in the other pan we inserted a thermo-couple probe to measure its temperature in the course of the experiment, see Supporting information **Figure S3**. We performed cooling and heating cycles, at rate of 0.5 °C/min, similar to those in the actual DSC experiments and in the observations with glass capillaries. We observed the same drop-shape transformations at the same temperatures in both experimental setups (with DSC pans and with optical capillaries). However, the images from the observations in reflected light with DSC pans are not as clear as those obtained with the glass capillaries, because the optical system is much superior in the latter experiment. Therefore, we use images from the experiments with glass capillaries to illustrate the observed drop-shape transformations.

Based on the fact that we observe the same drop-shape transformations in both types of experiment (with optical capillaries and with open DSC pans) we accept that the same transformations occur in the closed pans during the actual DSC experiments which are performed under the same conditions – same temperature range, same scan rate, etc.

Determination of the drop-size distribution in emulsions

The drop-size distribution in the studied emulsions was determined from microscope images. Drop diameters were measured using the Image Analysis Module of Axio Vision Software. More than 10,000 drops were measured in each sample and the mean volume-surface diameter $d_{32} = \sum_i N_i d_i^3 \Big/ \sum_i N_i d_i^2$ was determined (N_i is the number of drops with diameter d_i). We note that the mean drop size, d_{32}, appears in the estimates of the thickness of the layer of plastic rotator phase, h_{PL}, approximately as $1/d_{32}$, because we determine h_{PL} by comparing the ratio of the peak related to formation of rotator phase at the drop surface (proportional to d^2) and the peak related to the freezing of the entire drop content (proportional to d^3). Therefore, the final result depends on the specific surface area of the drops which is, by definition, proportional to $1/d_{32}$. As we measure d_{32} of the initial drops before starting the cooling-heating cycle in the DSC experiments or optical observations, we use hereafter the notation $d_{ini} = d_{32}$ of the initial drops, determined as explained above.

Illustrative histograms of the drop size distributions by number and by volume are presented in Supporting Information **Figure S4** for emulsions of hexadecane, stabilized by $C_{16}EO_{20}$ and $C_{16}SorbEO_{20}$ surfactants. From such histograms, demonstrating the narrow size distribution of the produced emulsions, we can estimate that the error introduced in the layer thickness by the inaccuracy of the measured d_{ini} is around 1% for the 9.5 and 33 μm drops and around 3.5 % for the smallest drops studied.

RESULTS AND DISCUSSION

In this section we present our results from the DSC measurements and connect them to the drop-shape transformations, observed by optical microscopy. Using the ratios between the areas of the enthalpy peaks in the DSC thermograms, we determine the fraction of the intermediate plastic rotator phase, formed in the course of emulsion cooling, prior to the complete freezing of the oily drops.

In the discussion below, we use the classification of the oil-surfactant systems, introduced in our previous study, Ref. 2. We classified the various surfactants into four distinct groups, depending on the onset temperature of drop transformation, T_d, as compared to the melting temperature of the bulk oil, T_m. Briefly, the surfactants which do not induce drop-shape transformations upon cooling belong to *Group D*. These are surfactants with too short hydrophobic tails and/or with very large head-groups. Therefore, their adsorption layers do not freeze at the surface of the cooled drop before the complete oil freezing inside the drops. As a

result, the adsorption layers of these surfactants are unable to trigger the formation of plastic rotator phase at the drop surface for the respective oil. In groups *A* to *C* we place surfactants which induce drop shape transformations upon cooling: surfactants in *Group A* are those for which $T_d > T_m$; *Group B* contains surfactants for which $T_d \approx T_m$, and *Group C* contains surfactants for which $T_d < T_m$; for more details see Ref. 2 and Supporting Information **Table S3**.

Below we show and discuss separately the experimental results, obtained with representative oil-surfactant pairs from these groups.

In **Figure 1** we present the DSC thermogram, obtained with hexadecane (C_{16}) drops for which $T_m \approx 18°C$, dispersed in $C_{16\text{-}18}EO_{50}$ surfactant solution. For this oil-surfactant pair, the surfactant falls into *Group D*, because it has very voluminous head-group of 50 ethoxy units and it does not induce drop shape transformations upon cooling.[2] As seen from the DSC curve, we observe one main peak with Gaussian shape, centered around 6ºC, and two small peaks around 15ºC.

In the microscope observations in capillary we saw freezing of a very small fraction of the oily droplets to start in the temperature range between 9.3 and 7.5 ºC, but the main fraction of the oil drops were seen to freeze around 6ºC, see **Figure 1b-d**. These optical observations can be directly related to the peaks in the measured DSC thermogram. As seen in **Figure 1**, the DSC signal starts to deviate slightly from the baseline at a temperature of 9-10ºC, while the main peak, caused by the bulk freezing of the emulsion drops, is observed at a temperature around 6ºC. The Gaussian shape of the main DSC peak is expected – although the drops are relatively monodisperse, the nucleation in the individual drops occurs at slightly different moments, resulting in a drop freezing within a certain temperature range, rather than at fixed temperature.[32-33]

The observations in a glass capillary did not show any sign of drop freezing at 15ºC. However, when we performed optical observations in a DSC pan, we observed multiple oil lenses floating on the surface of this particular emulsion sample, as well as some very big emulsion drops, **Figure 1e-g**. Both the oil lenses on the emulsion surface and the large emulsion drops were freezing at a temperature around 15 ºC. Thus, we conclude from these observations that the DSC peaks, observed around 15ºC, are due to crystallization of C_{16} in the large oil lenses and the large oil drops, at temperatures slightly lower than T_m, as a result of the moderate undercooling (by around 3ºC) of the oil in these large entities.

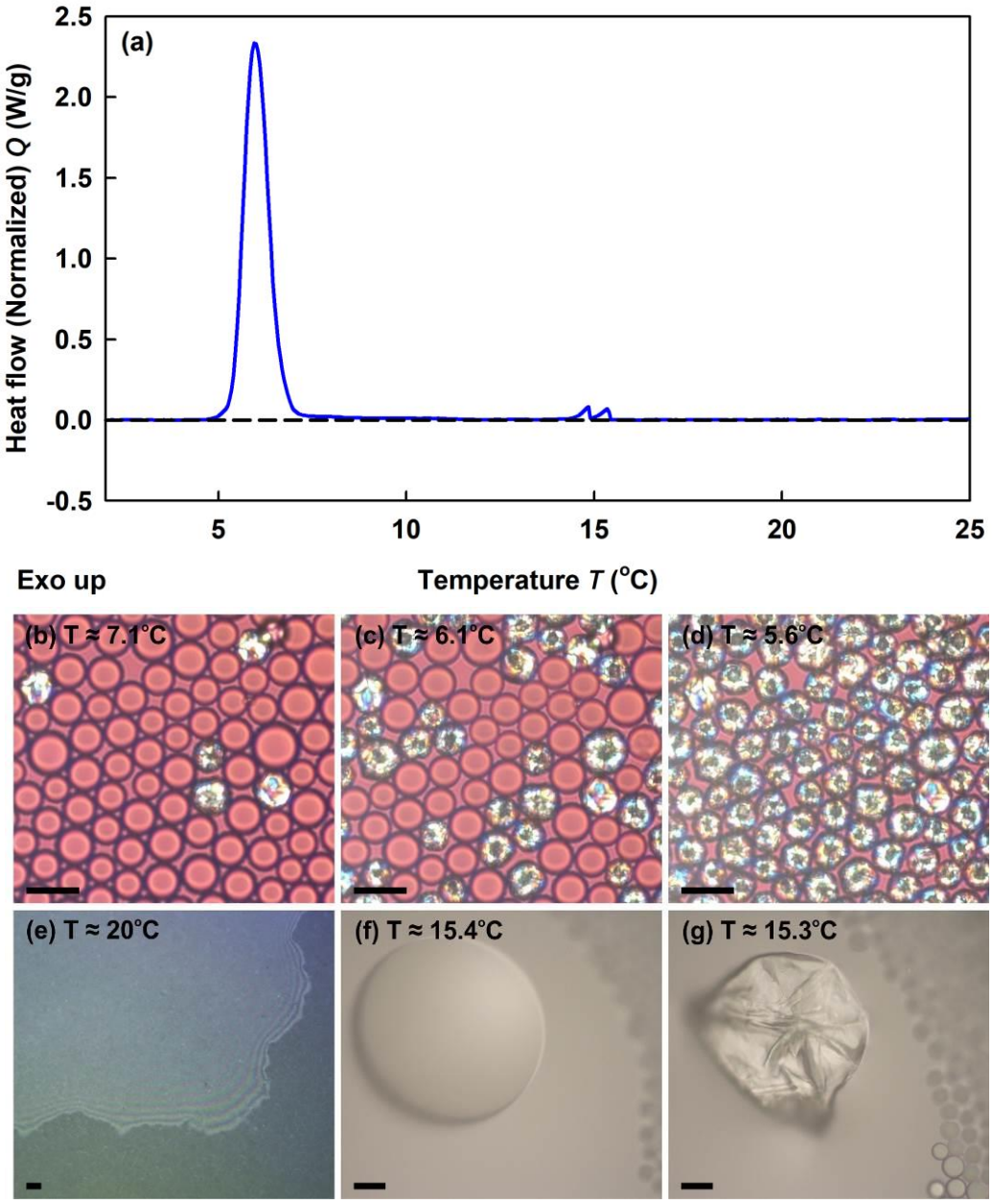

<u>Figure 1.</u> DSC thermogram and microscopy images for C_{16} drops with initial drop size, d_{ini} ≈ 10 µm, stabilized by $C_{16\text{-}18}EO_{50}$ surfactant (*Group D*). (a) DSC thermogram upon cooling; (b-d) Microscopy images in transmitted polarized light, showing the process of drop freezing upon cooling. The cooling experiment is performed in glass capillary. (b) The first freezing process is observed at temperature 9.3ºC, however as seen in this picture only a very small fraction of the drops has frozen down to 7.1ºC. (c-d) The main freezing process is observed between 6.5ºC and 5.6ºC. (e-f) Cooling experiment of the same sample, contained in a DSC pan. The drops are observed in reflected white light. The small peaks, observed in the thermogram around 15ºC are due to the freezing of the oil lenses and some large drops, formed after drop-drop coalescence. (e) Oil lenses are observed at the top of the sample, placed in a DSC pan. (f) Fluid big drop. (g) The drop freezes at a temperature 15.3ºC. All experiments (both DSC and optical observations) are performed at 0.5°C/min cooling rate. Scale bars, 20 µm.

Similar DSC results and explanations were reported by Shinohara and co-authors.[15] They present DSC data, obtained at a cooling rate of 2 ºC/min, for C_{16} drops with initial diameter, d_{ini} = 32.6 ± 3.2 μm, stabilized by 1 wt. % aqueous solution of Tween 20 surfactant ($C_{12}SorbEO_{20}$). This surfactant also belongs to *Group D*, according to our classification, because its C_{12} tail is by 4 carbon atoms shorter than the alkane chain-length. Therefore, this surfactant does not induce drop shape transformations upon cooling of hexadecane emulsions, as confirmed in our experiments. For this system, Shinohara and co-authors observed two exothermic peaks – one at 14.5 ºC interpreted as bulk C_{16} crystallization and a second broad peak with a maximum around 5.5 ºC, corresponding to crystallization of the alkane in the oily drops, see Figure 2 in Ref. 15. We also performed DSC and microscopy experiments with the same system - C_{16} drops, stabilized by $C_{12}SorbEO_{20}$ surfactant. The DSC results were very similar to those reported in Ref. 15. The optical observations of the emulsions in the DSC pan showed that oil lenses were formed on top of this sample as well, see Supporting Information **Figure S5**. The peak around 15ºC is associated with the freezing of these lenses.

We studied several other oil-surfactant pairs from *Group D* and observed the same phenomena with all of them. This type of behavior is caused by the fact that the surfactants in these emulsions do not form densely packed adsorption layers, due to their relatively short hydrophobic tail and/or relatively large hydrophilic head. As a result, the surfactants do not stabilize well the respective emulsions and oil lenses emerge on the emulsion surface and/or drop-drop coalescence is observed.[49] The formed larger entities (oil lenses/drops) freeze at temperatures around and slightly below T_m, while the main fraction of the drops freeze at much lower temperature, without undergoing drop-shape transformations. Formation of oil lenses and/or huge emulsion drops was not observed for any of the other tested systems from *Groups A-C*.

Group B: Surfactants which induce drop self-shaping at $T_d \approx T_m$

The data interpretation for surfactants inducing drop-shape transformations is most straightforward for the surfactants from *Group B*. Therefore, we present first the results for an emulsion which is representative for this type of systems: C_{16} drops with $d_{ini} \approx 9.5 \pm 0.1$ μm, stabilized by $C_{16}SorbEO_{20}$. The respective DSC curve and microscopy images are shown in **Figure 2**.

Before discussing the results for this system, we should emphasize that we do not observe any measurable peaks in the cooling DSC thermograms of the surfactant solution of $C_{16}SorbEO_{20}$ without dispersed oil, see Supporting Information **Figure S6**. No peaks are

observed in the temperature interval 0-30°C also for emulsions containing drops of shorter-chain alkanes (e.g C_{12}), stabilized by a long-chain surfactant in which the oil drops freeze at much lower temperatures, see Supporting Information **Figures S7**. Thus, we can conclude that all peaks observed in the thermograms presented below are due entirely to the enthalpy release upon ordering of the alkane and surfactant molecules in the emulsion drops, viz. these peaks do not contain any enthalpy contribution generated by changes in the surfactant aggregates (micelles) in the aqueous phase.

The cooling thermogram of C_{16} drops dispersed in $C_{16}SorbEO_{20}$ solution shows four major exothermic peaks, **Figure 2a**. The first peak starts sharply at 15.2 ± 0.2ºC (data from 4 independent measurements), for this particular sample the peak starts at 15.4ºC and returns back to the baseline at 14.8 ºC. The second peak starts from around 14ºC and continues down to 11ºC where the third major peak starts to develop. The third and the fourth peaks largely overlap and return back to the baseline at 5 ºC. The total area of these peaks corresponds to the total enthalpy of complete freezing of the dispersed alkane. The freezing of all drops at the lowest temperature is confirmed by optical observations. Therefore, by comparing the measured enthalpy in the emulsion experiments to the enthalpy of freezing of pure hexadecane (≈ 235 J/g),[9] we can calculate the actual oil weight fraction, Φ, in the emulsion studied:

$$\mathbf{\Phi} = \frac{H_{m,\,emulsion}}{H_{m,\,bulk\ oil}} \tag{1}$$

We note that we do not use the calculated oil weight fraction anywhere in the data interpretation. We always use the ratio between the enthalpy peaks measured in specific temperature range upon cooling, and the total enthalpy of drop melting measured upon heating of the same sample. Typical emulsion heating thermograms are presented as **Figure S8** in the Supporting information.

The two overlapping peaks at the lowest temperature in Figure 2a correspond to the complete freezing of the deformed hexadecane drops into crystalline phase, cf. **Figure 2f,g**. Note that the temperature of the rotator-to-crystal phase transition differs significantly from the temperature of the liquid-to-crystal phase transition only for the alkanes with thermodynamically stable (or metastable) bulk rotator phase, like that in the interior of the mixed alkane drops.[12,50] The rotator phase in bulk hexadecane is thermodynamically classified as “transient” and it is very short leaving.[12] Therefore in **Figure 2a**, we do not observe a separate rotator-to-crystal phase transition from the liquid-to-crystal phase transition inside the interior of the hexadecane

drops – the first formation of true crystal phase in the drops acts as a nucleus for the complete crystallization of the hexadecane drop interior into the final, truly crystalline form.

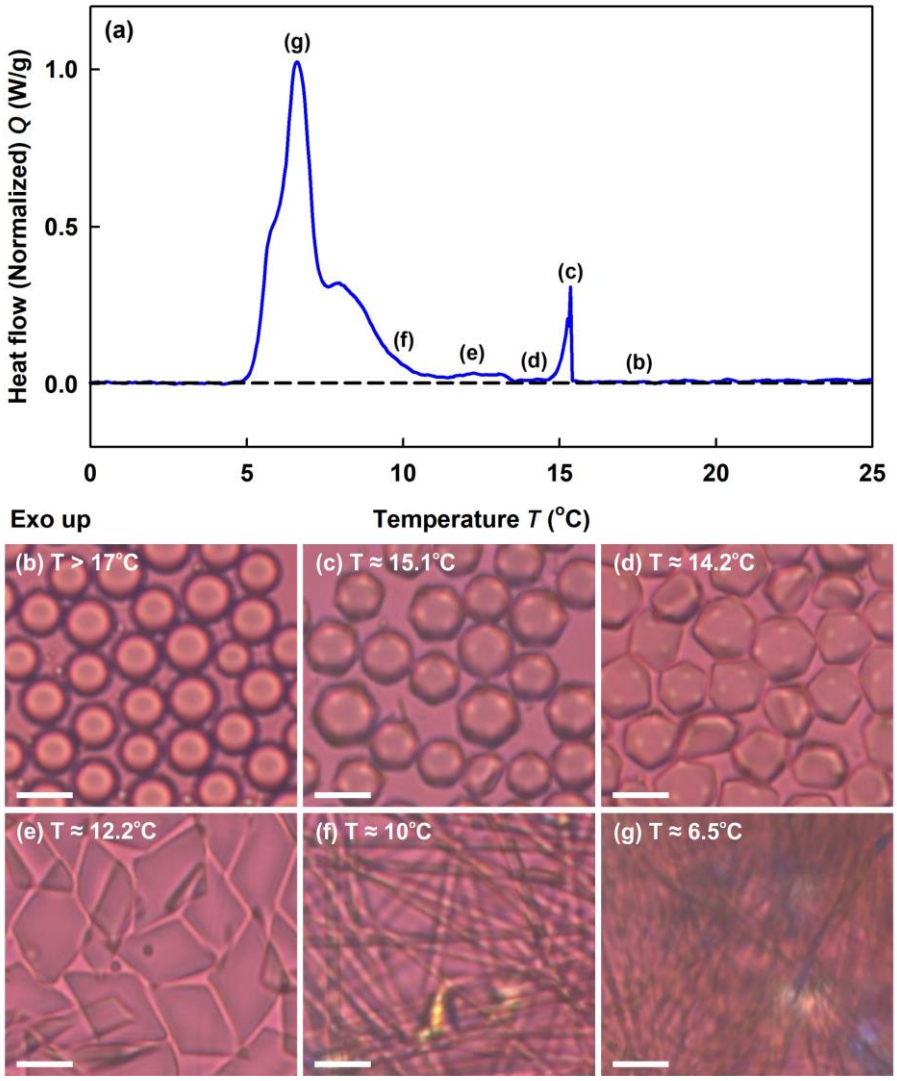

Figure 2. DSC thermogram and microscopy images for C_{16} drops with $d_{ini} \approx 9.5 \pm 0.1$ µm, stabilized by $C_{16}SorbEO_{20}$ surfactant (*Group B*). (a) DSC thermogram, obtained at 0.5 °C/min cooling rate; (b-g) Microscopy pictures showing the different stages of the drop shape evolution upon cooling; cooling rate 0.5 °C/min. (b) All emulsion drops are spherical at temperatures above 17ºC. (c) Drop shape transformations start around 15.2 ± 0.2ºC (data from 4 independent measurements), for this particular sample the peak starts at 15.4ºC. At this temperature the DSC curve starts to deviate from the baseline. (d) At temperature around 14.2ºC flattened polyhedrons are formed. (e) The decrease of the temperature leads to further evolution in drop shape. At temperature around 12.2ºC, drops have evolved up to the stage of tetragonal platelets. (f) Some rare drops were observed to freeze at 11ºC ≤ T ≤ 12ºC, while most of the drops elongate into long fibers. (g) The thin elongated fibers freeze (crystallize) completely at $T \approx 6.5$ºC. Scale bars, 10 µm.

On the other hand, we do not observe any freezing (crystallization) of the drops in these emulsions down to 12 ºC – neither in the capillary experiments nor in the DSC pan experiments. Therefore, the peaks observed above 12 ºC, are related entirely to enthalpy released in the process of molecular rearrangement of the hexadecane in the non-frozen oil drops (with a possible contribution from the freezing surfactant adsorption layer). Let us relate now these peaks to the observed shape transformations in the deforming drops, **Figure 2**.

The highest-temperature peak appears at the temperature, at which we observe the initial drop-shape changes. As seen in **Figure 2c**, at a temperature of 15.1ºC all drops have evolved into regular polyhedrons. Thus we conclude that the first peak is related to the process of polyhedron formation. The second peak corresponds to the next stages of the drop shape evolution, in which the polyhedrons flatten and hexagonal platelets are formed, cf. **Figure 2d**. Upon further cooling, the drops transform into tetragonal platelets. The subsequent stage is elongation of the tetragons and their transformation into thin fibers. However, some drops freeze in the shape of elongated prisms, before transforming into fibers, cf. **Figure 2f**.

The enthalpy, measured from the beginning of the drop shape transformations up to the formation of tetragonal platelets at temperature of 12.2ºC, is around 3.8 % ± 0.6 % from the total enthalpy measured in the whole DSC experiment (average from 4 independent measurements), see also Supporting information **Figure S8**. This means that ≈ 3.8 % of the total enthalpy has been released along the transition from isotropic liquid phase into a phase with higher order, before any freezing of the oily drops is observed. From the optical observations, we can calculate the average geometric parameters of the platelets formed at this temperature, see **Figure 3a**. The side lengths of the platelets are 12.5 ± 2 μm, while their obtuse angle is 120 ± 8º. The three dimensional shape of the platelets is shown schematically in **Figure 3b**. For the following estimate, this shape can be approximated in the following way: the periphery of the platelet is approximated with a cylinder of radius, *r*, while the volume of the inner part of the platelet is represented as a plane-parallel platelet, **Figure 3c,d**. As the drops change their shape at fixed drop volume, the average thickness of this central part of the tetragonal platelets can be calculated from the volume conservation principle, see **Supporting Information Section 1** for more details. Thus, from the measured geometrical parameters and the enthalpy of the tetragonal platelets, we can estimate the thickness of the new phase, formed at the drop surface in the process of drop-shape transformation. We have made these estimates using two different assumptions to capture the upper and the lower boundaries of the rotator phase thickness:

As an upper limit for the estimate of the thickness of the formed rotator phase (Model I), we assume that the latter is formed only at the platelet periphery (along the curved perimeter

edges), while no rotator phase is formed on the flat surface in the central part of the platelet, **Figure 3c**. This assumption is supported by the symmetric drop breakage observed upon cooling of such platelets[7,8] – indeed, if rotator phase was formed in the central region, it would stabilize the particles against puncturing of the platelet in this central region. Under this assumption, the volume of the formed rotator phase, V_{PL}, may be estimated as explained in Supporting Information, Section 2a. In these estimates important parameters are the thickness of the plastic (rotator) phase, h_{PL}, and the thickness of the plane-parallel body in the particle center, h_m, which may vary in the general case between $h_m \to 0$ (very thin central part) and $h_m \approx 2r$ (flat platelet) in this consideration, see **Figure 3c**. The fraction of the formed rotator phase (compared to the total drop volume) is equal to the ratio of the enthalpy released down to the temperature at which the deformed drop is analyzed and the total enthalpy of complete drop freezing, corrected by a constant, k:

$$\frac{V_{PL}}{V_{total}} = \frac{k\,H_{PL,\ down\ to\ T=12.2^{o}C}}{H_{total}} \approx 0.038k\,, \qquad (2)$$

where 0.038 = 3.8 % is the measured fraction of the total enthalpy. The parameter k takes into account the fact that the enthalpy of formation of the rotator phase (per molecule) is a fraction of the total enthalpy of complete freezing of the molecules included in the rotator phase. This parameter represents the ratio between the enthalpy of formation of the crystalline phase to the enthalpy of formation of the rotator phase, in both cases starting from liquid phase, for the same alkane amount. From the literature data[9] we know that the enthalpy of formation of the rotator phase is around 80% of the total enthalpy of complete oil freezing for pentadecane and heptadecane. Therefore, we assume $k \approx 1/0.8 = 1.25$ in our estimates. The total volume $V_{total} = \pi d_{ini}^3/6$, is the volume of the initial drop. Substituting the experimental parameters in eq. 2, we can estimate the fraction of the rotator phase formed. As average values from our measurements we take $d_{ini} = 9.5 \pm 0.1$ μm. The value of h_m may vary significantly during the cooling process. In order to estimate the thickness of h_{PL}, we assumed a certain ratio for the thickness of the middle platelet over the cylinder radius, h_m/r, and checked which value of the thickness of the rotator phase would satisfy the equation for the rotator phase volume (equation S10 in Supporting information), while the values of h_m and r satisfy simultaneously equation for the total platelet volume (equation S6 in Supporting information). In this way we determined the possible variation of h_{PL} which satisfies all experimentally determined quantities, in the range of reasonable values of the ratio $0 < h_m/r \leq 2$. From these calculations we found that the h_m varies in range between 0.4 μm for $h_m = 0.2r$ and 3.2 μm for $h_m = 1.9r$. Respectively, the values of r vary

between 2 and 1.7 μm. The mean value of h_m for the whole range is 1.8 ± 1.2 μm, while for r it is 1.85 ± 0.3 μm. Performing these calculations, we found that the thickness of the plastic phase falls in the range between 49 ± 5 nm for $h_m = 0.2r$ and 70 ± 5 nm for $h_m = 1.9r$. The standard deviations are calculated by making calculations for more than 15 deformed drops using each of the above assumptions. Thus, we see that the most probable value of h_{PL} is around 55 ± 15 nm, where the standard deviation accounts also for the uncertainty in the values of h_m. Further variations of h_m in the entire range between 0 and $2r$ do not change this main result of the calculations and the related conclusions. The lamellar spacing for hexadecane molecules in pseudo-hexagonal rotator phase is 2.26 nm,[13] which means that the estimated thickness corresponds to a multilayer of ≈ 24 ± 6 parallel layers of ordered hexadecane molecules, corresponding to the range between 18 and 30 ordered alkane layers.

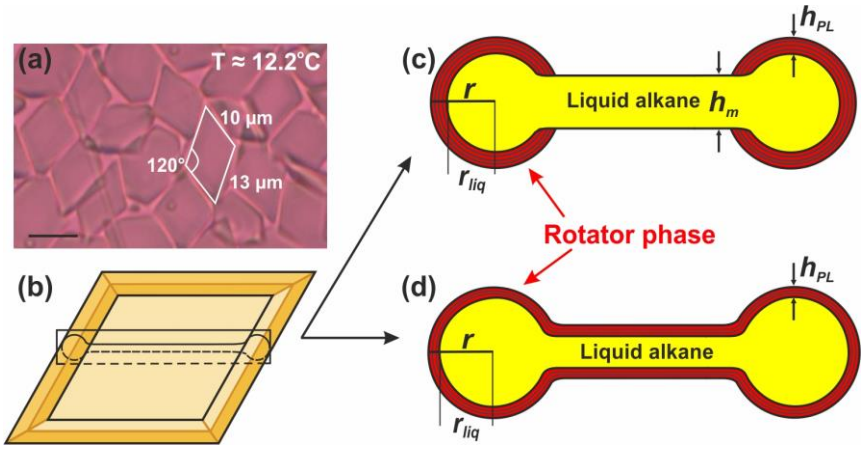

Figure 3. Calculation of the rotator phase thickness for tetragonal platelets (*Group B*). (a) Microscopy image of fluid tetragonal platelets obtained upon cooling of C_{16} emulsion sample stabilized by $C_{16}SorbEO_{20}$ surfactant. The initial drop size is $d_{ini} \approx 9.5$ μm, drops are cooled at 0.5 °C/min. Scale bar, 10 μm; (b) Sketch of a fluid platelet; (c-d) Sketches of two alternative models used to estimate the thickness of the rotator phase, formed at the platelet surface: (c) Model I: Geometrical model in which it is assumed that the rotator phase is formed only at the platelet periphery (in the regions of high interfacial curvature) while the alkane in the inner part of the drop is in a liquid state; (d) Model II: Geometrical model using the assumption that a homogeneous layer of rotator phase is formed over the entire surface of the deformed drop. See text for more details.

To estimate the lower limit of the rotator phase thickness from the measured DSC peak areas, we adopted an alternative assumption (Model II) – namely, that a homogeneous layer of rotator phase is formed over the whole surface of the platelet, **Figure 3d**. We should note that the available experimental results do not support this assumption. Nevertheless, it could be used to

find the minimal possible thickness of the rotator phase in these emulsions. Under this assumption, $V_{PL} = Sh_{PL}$, where S is the surface area of the platelet. The total volume of the rotator phase and the related thickness h_{PL} in this model are estimated as explained in **Supporting Information Section 2b**. Using the same assumptions as in the previous model, with the same r values which vary between 1.7 and 2 μm, we estimated the thickness of the rotator phase to fall in the range between 40 ± 7 nm for $h_m = 0.2r$ and 51 ± 6 nm for $h_m = 1.9r$. Thus we see that the most probable value of h_{PL} in this model is around 45 ± 13 nm.

Similar, though less precise estimate could be made for the thickness of the rotator phase, formed at the very early stage of polyhedrons formation, **Figure 2c**. For this estimate we assume that homogeneous rotator phase is formed on the entire surface of the polyhedrons and the respective enthalpy is reflected only in the first peak, observed at around 15ºC. Thus we estimated the thickness of the rotator phase to be ≈ 36 nm for assumed icosahedral shape of the deformed drop and ≈ 32 nm for assumed octahedral drops. The latter, very close values show that this estimate is weakly affected by the assumed specific shape of the polyhedrons. Furthermore, the agreement in the values for h_{PL} with the estimate performed above for the platelets, shows that all these estimates are robust with respect to specific details in the assumptions made.

DSC and microscopy experiments were performed also with smaller emulsion drops, d_{ini} ≈ 3 μm, from the same emulsion system: C_{16} drops, dispersed in $C_{16}SorbEO_{20}$ surfactant solution. The DSC curve and the respective microscopy images are shown in **Figure 4**. The main observed difference between the two latter systems (9.5 μm vs. 3 μm drops) was in the kinetics of the drop shape evolution, as explained in Ref. 2. The smaller drops evolved much faster, viz. for shorter time under otherwise equivalent conditions, up to the last stages of the evolutionary scheme, forming triangular platelets and long thin fibers, **Figure 4d-f**.

The DSC curve, obtained with these smaller drops, starts to deviate sharply from the baseline at a temperature of 15 ± 0.3 ºC (data from 10 independent measurements), for this particular sample the deviation starts at 14.7 ºC and the maximum of the first peak is at 14.6 ºC, cf. **Figures 4a** and **4d**. The microscopy observations showed that the drops started to deform around 17 ºC where the small deviation from the baseline does not allow us to measure reliably the initial enthalpy effects, see **Figure 4c**. The first observed peak at ≈ 15°C corresponds to the drop shape transformation from regular polyhedrons into long rods and trigonal platelets, **Figure 4d**. These trigonal platelets freeze at a temperature of around 13.5ºC, **Figure 4e**, while the rod-

like droplets elongate further into thin fibers and freeze completely at a much lower temperature, around 5.5ºC, **Figure 4g**.

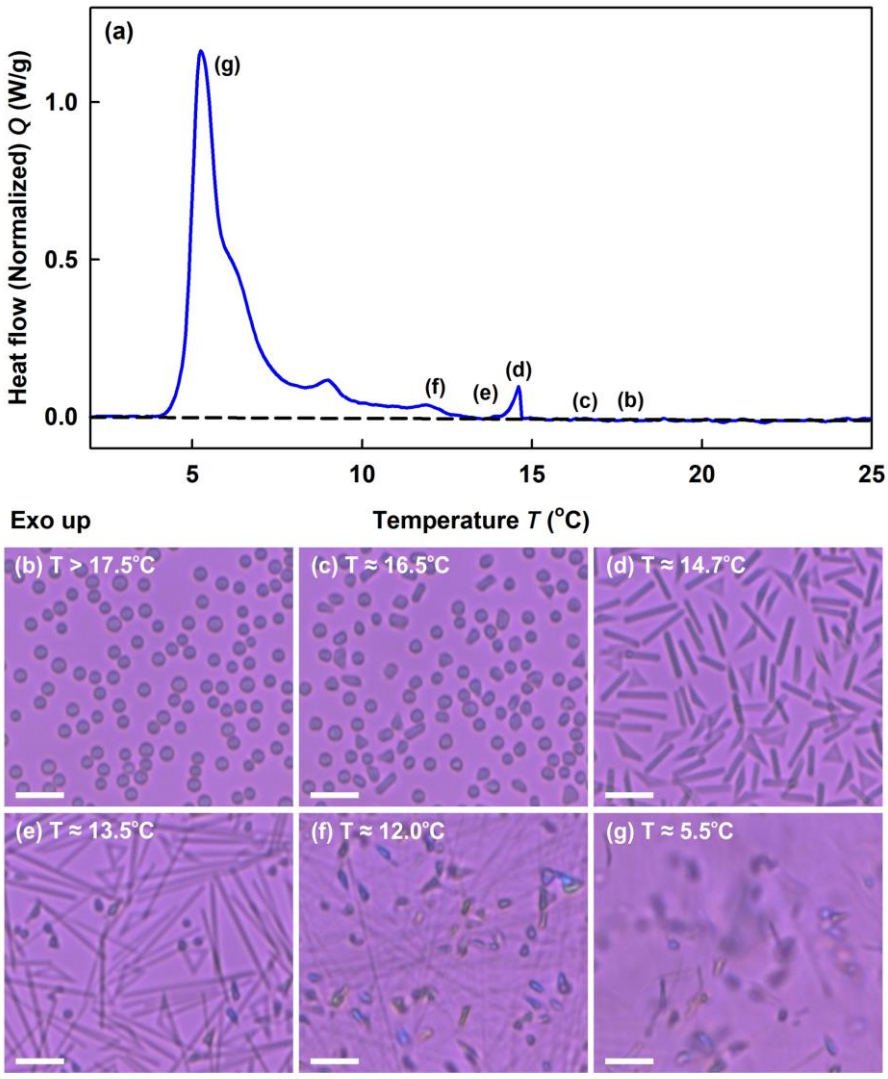

<u>Figure 4.</u> DSC thermogram and microscopy images for C_{16} drops, d_{ini} ≈ 3 µm, stabilized by C_{16}SorbEO$_{20}$ surfactant (*Group B*). (a) DSC thermogram, obtained at 0.5 °C/min cooling rate; (b-g) Microscopy pictures showing the different stages of the drop shape evolution upon cooling; cooling rate 0.5 °C/min. (b) All emulsion drops are spherical at temperatures above 17.5ºC. (c) Significant drop shape transformations start in the range between 17 and 15 ºC. The initial weak deviation of the DSC curve from the baseline is followed by a sharp deviation at 15 ± 0.3 ºC (data from 10 independent measurements), for the thermogram presented on the figure, the curve deviates sharply at 14.7 ºC. (d) At temperature around 14.7ºC rod-shaped entities are formed. (e) At temperature around 13.5ºC the drops have evolved into long rods and first drop freezing is observed. (f) Thin fibers are formed around 12ºC, along with additional drop freezing. (g) All thin fibers freeze at temperature around 5.5ºC drops. Scale bars, 10 µm.

From these results, we can calculate the thickness of the rotator phase in the thin fibers like those shown in **Figure 4d**. By integrating the DSC peak down to 13.8ºC, we calculated that the enthalpy of formation of the fibers with length of around 15.2 ± 2.3 μm is around 2.7 % ± 0.8 % of the total enthalpy of all peaks (data from 10 independent experiments). In this case, the ratio of the volume of the rotator phase to the total drop volume can be expressed as:

$$\frac{V_{PL}}{V_{total}} = \frac{k\,H_{PL,\ down\ to\ T=13.8^{o}C}}{H_{total}} \approx 0.027k \qquad (3)$$

where the constant k = 1.25 has the same meaning and value as in eq. 2. To estimate the thickness of the rotator phase formed on the fiber surface, we assume that it is formed along the surface of the whole fiber and has uniform thickness. Thus we model the fibers as two coaxial cylinders with different radii, the inner cylinder with radius r_{liq} is filled with isotropic liquid oil, while the space between the outer (with radius r) is occupied by plastic rotator phase, **Figure 5**.

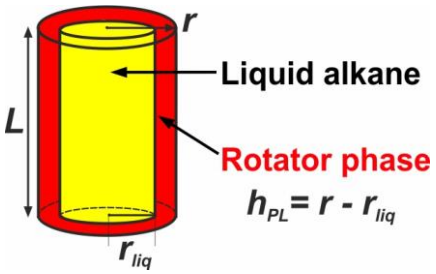

<u>Figure 5.</u> Calculation of the rotator phase thickness for the rod-like fluid drops (*Groups B and C*). Sketch of the geometrical model used for calculation of the rotator phase thickness in rod-like fluid drops. The rotator phase is formed with homogeneous thickness on the drop surface, while the core of the drop contains isotropic liquid (see text for details).

As illustrated in **Figure 5**, the volume of the liquid phase is $V_{liq} = \pi r_{liq}^2 L$, the volume of the plastic phase is $V_{PL} = \pi L\left(r^2 - r_{liq}^2\right)$ and the total volume is $V_{total} = \pi d_{ini}^3/6 \approx \pi r^2 L$, where L is the length of the rod-like particle. In the last equation we have neglected the volume of the two hemispherical caps at the rod ends, because the ratio $r/d_{ini} << 1$. Using these relations and the fact that the rods at this moment are around 15 μm long, we calculate the thickness of the rotator phase, $h_{PL} = r - r_{liq}$, to be around 9.4 ± 3 nm, corresponding to a multilayer of around 4 ± 1 molecules thick.

We did not try to determine h_{PL} for the drop shapes in the earlier stages of the drop evolution, shown in Figure 4, because the molecular layers might be distributed non-homogeneously on the drop surface for the more complex drop shapes and such an estimate would inevitably involve some speculative assumptions.

In conclusion, the experiments performed with C_{16} drops, stabilized by $C_{16}SorbEO_{20}$ surfactant (*Group B*), show unambiguously that the drop shape transformations in this system are caused by the formation of multilayers of ordered alkane molecules. The thickness of the layers varies between ≈ 10 nm for the smallest studied drops which transform into thin fibers and ≈ 55 ± 15 nm for the intermediate in size drops which transform into tetragonal platelets.

Group C: Surfactants which induce drop self-shaping at $T_d < T_m$

Similar experiments were performed with hexadecane drops with initial diameter, d_{ini} ≈ 2.6 μm, stabilized by $C_{16}EO_{20}$ surfactant. This is a surfactant from *Group C* in our notation, because the drop-shape transformations start at $T_d < T_m$, see Supporting information **Table S3**. The DSC curve and the respective microscopy images are shown in **Figure 6**. As expected, the first deviation from the baseline in the DSC signal is observed at ≈ 10.5ºC, when the drop shape transformations start. The thermogram has two exothermic peaks, one broad peak from 10.5ºC to 6.5ºC and a second peak with higher intensity between 6.5 and 4ºC. From five independent samples, we calculated that the enthalpy of the first peak is around 16.5 ± 1.2 %, while the second peak has enthalpy around 83.5 % from the total enthalpy. This second peak corresponds to the final freezing of the droplets, see **Figure 6g.** The Gaussian shape of this peak is expected, because all drops that had not been frozen until that temperature had transformed into long fibers with very similar shape and dimensions and, therefore, all they freeze at similar temperatures.

The interpretation of the first peak is not straightforward. As seen in **Figure 6d**, almost all drops have evolved in shape into short rods at T ≈ 9.8 ºC. However, two of the particles in this image had frozen at an earlier stage of their evolution. Statistical analysis over > 2 500 drops showed that 8 ± 2 % of the drops in these emulsions freeze at temperature around 10ºC, while the rest of the dispersed entities evolve into the later stages of the evolutionary scheme and freeze around 5-6ºC. On the other hand, the enthalpy of the first peak (16 %) is about two times larger than that originating from the drops frozen at this stage (8 % frozen drops). Therefore, we can conclude that about half of the first peak is due to the enthalpy released around 10ºC in the process of drop deformation without alkane freezing. In other words, about 8 % of the enthalpy is due to the formation of ordered multilayers of alkane molecules in a rotator phase, causing the drop shape transformations.

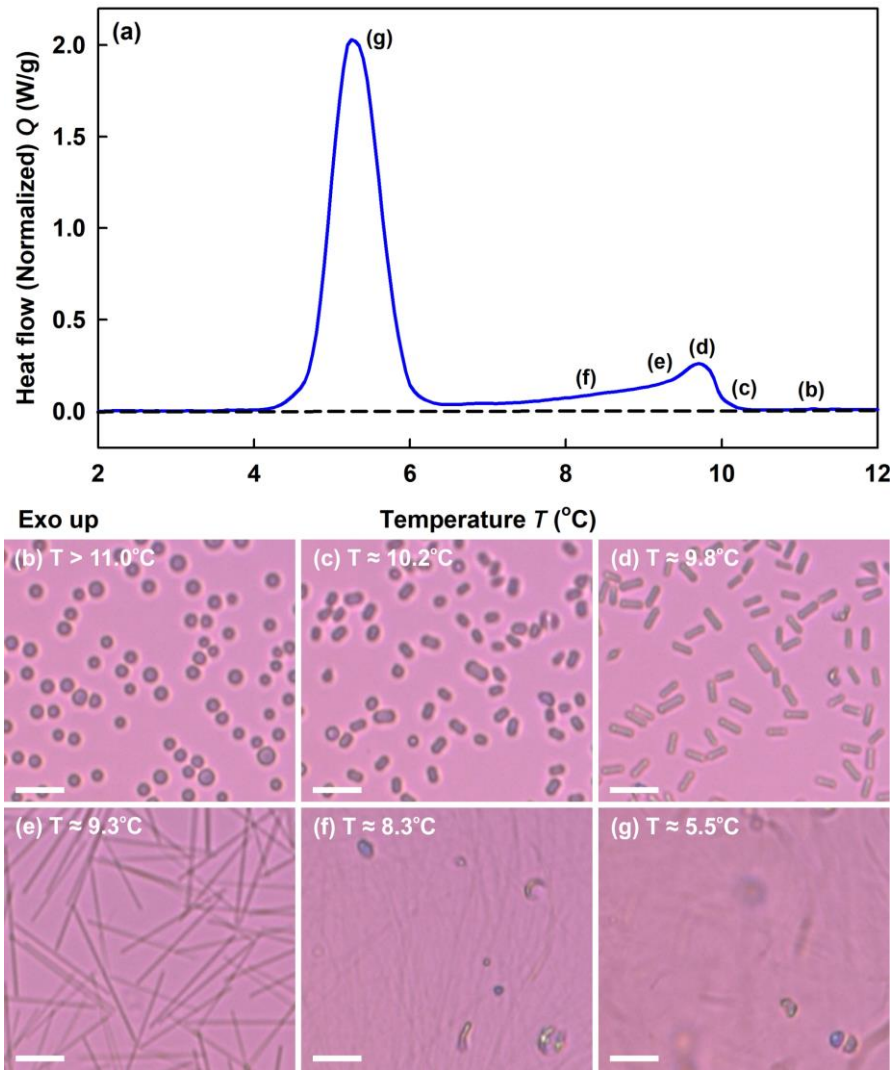

Figure 6. DSC thermogram and microscopy images for C_{16} drops, d_{ini} ≈ 2.6 μm, stabilized by $C_{16}EO_{20}$ surfactant (*Group C*). (a) DSC thermogram, obtained at 0.5 °C/min cooling rate; (b-g) Microscopy pictures showing the different stages of the drop shape evolution upon cooling; cooling rate 0.5 °C/min. (b) All emulsion drops are spherical at temperatures above 11ºC. (c) Drop shape transformations start around 10.5ºC and drops rapidly evolve into short rods. At this temperature the DSC curve starts to deviate from the baseline. (d-e) With the decrease of the temperature, the rod length increases, while the diameter decreases. (f) Thin long fibers are formed from the rods. Some colored frozen drops are seen which had been frozen at higher temperatures, ca. at $T \approx 10$°C. (g) Freezing of the fibers. At this temperature the second peak in the DSC thermogram is observed. Scale bars, 10 μm.

This data interpretation is supported also by the fact that the first peak in the thermogram is observed throughout a wide temperature range, from 10.5 down to 6.5ºC, and the DSC curve returns to its baseline only after the final freezing of all drops, see the punctured black line in

Figure 6a. However, an initial freezing of the drops happens around 10ºC only, whereas no further freezing (crystallization) of drops is observed between 10 and 6.5ºC, because all drops that had acquired rod-like shape did not freeze down to 5-6ºC, see **Figure 6c-f**. This means that the DSC signal observed between 10 and 6.5ºC is entirely associated with the drop-shape transformations, observed in this temperature range. From the area of this peak, assuming that the rotator phase is formed as a thin layer over the entire surface of the rod-shaped droplets (same assumption as that shown in **Figure 5**), we estimated the thickness of the rotator phase as 8 ± 2 nm (viz. 3 ± 1 alkane layers). For this estimate we used d_{ini} = 2.6 μm and $L \approx 120$ μm. The fiber length was estimated from the diameters of the drops formed after one freeze/thaw cycle in this emulsion system. As explained in Ref. 7, the diameter of the drops formed after fiber melting via Rayleigh-Plateau type of instability, is around 1.9 times bigger than the diameter of the fibers from which they have been formed. As shown in Ref. 7, the drop diameter after one freeze/thaw cycle in this emulsion is around 600 nm (by number), i.e. these drops are formed from fibers with diameter of ≈ 315 nm which corresponds to $L \approx 120$ μm.

Group A: Surfactants which induce drop self-shaping at $T_d > T_m$

To complete this study with all different types of surfactant, here we present our DSC and microscopy results for the surfactants which induce drop-shape transformations at $T_d > T_m$, viz. for the surfactants from *Group A*. The studied emulsions contained C_{16} drops with $d_{ini} \approx 33$ μm, stabilized by $C_{16}EO_{10}$ surfactant. In this system, the drop-shape transformations start at ≈ 23ºC, while the drop freezing is observed predominantly in the range between 14 ºC and 15 ºC. The drops in this system behaved differently compared to the systems discussed in the previous paragraphs – first, polyhedrons with irregular shape and corrugated surface are formed and several subsequent breakage events are observed upon cooling, see **Movie S1**. After each breakage event, several smaller drops are formed while the main fraction of the oil remains in the central ("mother") drop.[8]

Two DSC thermograms, measured independently with this system, are presented in **Figure 7a,b**. As seen in **Movie S1** and in **Figure 7d**, the drop-shape transformations start well above the temperature at which the process of freezing is observed (≈ 15°C). The first drops start to change their shape at a temperature around 22.5ºC, but the massive drop transformations are observed in the temperature range between 22 and 21 ºC. As expected, in the range 21 to 22 ºC, the DSC curve significantly deviates from the baseline well above the noise signal, forming small but well reproducible and non-negligible peak. This peak was observed with all tested

samples (more than 3) from this type of emulsion. At temperatures below this peak we observe continuous exothermic deviation of the DSC curve above the baseline which reflects the continuous drop shape transformations in this temperature range.

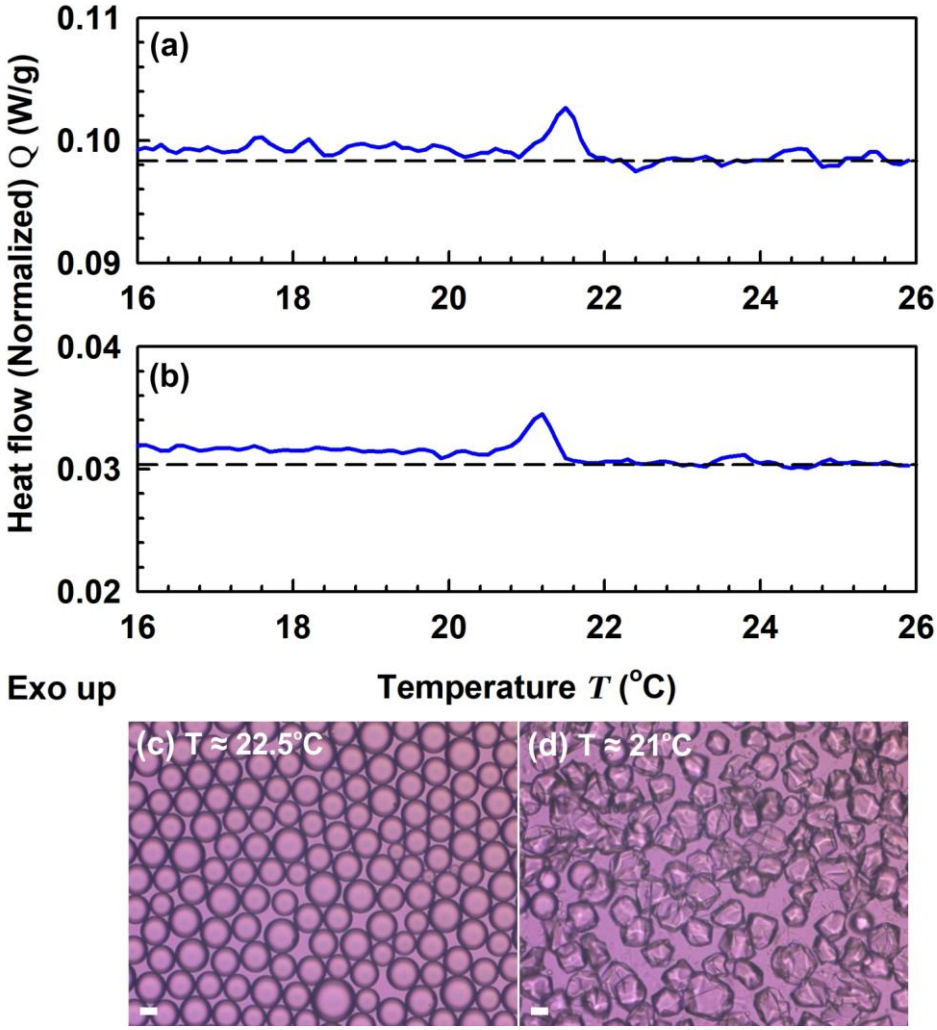

<u>Figure 7.</u> DSC thermogram and microscopy images for C_{16} drops, d_{ini} ≈ 33 µm, stabilized by $C_{16}EO_{10}$ surfactant (*Group A*). (a-b) DSC thermograms, obtained at 0.5 °C/min cooling rate from two independent measurements for the temperature interval between 16 and 26ºC. Note that although the peak observed between 20 and 22ºC is relatively small, it is well reproducible. Furthermore, the curve stays above the baseline value at T < 22 °C which reflects the continuous drop shape transformations in this temperature range. (c-d) Microscopy pictures showing the different stages of the drop shape evolution upon cooling; cooling rate 0.5 °C/min. (c) Most of the drops are spherical at temperatures above 22.5ºC, **see Movie S1**. (d) All of the drops have changed their shape at 21 ºC. The thermograms are rescaled only with respect to the oil weight fraction, the baselines have not been shifted to "zero" value.

To estimate the rotator phase thickness in these emulsions, we used two alternative assumptions. The first assumption is that a rotator phase with uniform thickness is formed on the entire drop surface. This assumption allows us to calculate the lower limit of the rotator phase thickness. As the initially formed shapes are irregular, we cannot calculate precisely their surface area. Therefore, to estimate approximately the realistic range of surface areas of these drops we calculated the surface area of several polyhedrons having the same volume. Assuming that the spherical drop is transformed into regular polyhedron (icosahedron, octahedron or cube), we found that the surface of the deformed bodies increases by less than 25 %, as compared to the initial spherical surface. Therefore the thickness of the rotator phase is bound within the limits $V_{PL}/S_{IN} \geq h_{PL} \geq V_{PL}/1.25S_{IN}$, where the S_{IN} is the surface area of the initial spherical drop. Comparing the volume of the rotator phase to the total volume and the areas of the peaks from the thermogram, we obtained that the thickness of the plastic phase is 6.25 nm ≥ h_{PL} ≥ 5.00 nm (2-3 layers). In this estimate we used d_{ini} = 33 μm, k = 1.25 and enthalpy ratio (H_{PL}/H_{total}) ≈ 9.1×10^{-4}, as measured experimentally.

Alternatively, if we assume that the rotator phase is formed not as a homogeneous layer on the entire surface of the polyhedral entities, but on the edges of the polyhedrons only (assumption which corresponds much better to our explanation[1-4] for the origin of the drop shape transformation), then we estimated that the rotator phase would be with thickness that is much larger, between ca. 30 nm and 180 nm, depending on the specific assumptions made. This range of h_{PL} values was estimated assuming icosahedral shape of the deformed drops and some additional assumptions for the specific shape of the strips of rotator phase, formed along the edges of the icosahedral drop, see Section S3 of the Supporting Information for detailed explanations. Two theoretical models have been tested to make these estimates and both models gave similar results, as described in Section S3 of the SI. Therefore, for the emulsions stabilized by surfactants from *Group A* we cannot make a final conclusion about the thickness of the rotator phase, until we have additional experimental information about the distribution of the rotator phase on the surface of the polyhedrons. Nevertheless, we conclude that neither of the performed realistic estimates could explain the drop shape transformations as a result of freezing of the adsorption monolayer only.

Thus, we can conclude from all performed experiments that the enthalpy of the peaks, observed before the complete freezing of the alkane drops, is related to formation of multilayers of ordered alkane molecules on the drop surface for all systems studied. The thickness of these

multilayers depends significantly on the specific surfactant-oil pair. Some of the results indicate that the thickness of the multilayer depends on the size of the deforming droplets as well.

THICKNESS AND MECHANICAL STRENGTH OF THE LAYERS OF ROTATOR PHASE

To preserve the observed characteristic curvature with radius $r \approx 1$ μm at the edges of shaped droplets, at a finite interfacial tension, γ, we need to overcome the capillary pressure which would otherwise unfold the shapes into spherical drops with minimal surface energy. The balance of the bending moments created by the interfacial tension and the plastic rotator phase requires that the bending elasticity constant of the plastic phase formed at the surface of the shaped drops should satisfy the relation:[1-3]

$$K_B \geq \gamma r^2 \tag{4}$$

where K_B is the bending elasticity constant of the interface (including the multilayers of the rotator phase).

In our original papers[1-3,16] we estimated the thickness of the layers of rotator phase, able to deform the surface of the oil droplets with interfacial tension of ≈ 5 mN/m, as being of the order of 15 to 300 nm. This estimate was based on the model by Evans[51] which analysed the variation of the free energy of bio-membranes and of interlocked multilayers of lipids upon their bending deformation. Assuming zero shear resistance of the molecular layers in the multilayer structure, Evans[51] found a quadratic dependence of the bending elasticity constant, K_B, of membrane layers on their thickness, h:[51-52]

$$K_B \approx K_{B1}(h/h_1)^2 \tag{5}$$

where h_1 is the thickness of the contained monolayers and K_{B1} is their individual bending modulus. For frozen (rigid) monolayer of surfactant/lipid/alkane molecules with thickness $h_1 \approx 2$ nm the bending modulus K_{B1} is in the range between 10^{-18} and 10^{-17} J.[17-19]

In his original study, Evans acknowledged[51] that the biological membranes have non-zero shear modulus, but also suggested that the respective contribution to bending is small enough to disregard it. The scaling expressed via eq. 5 has been used successfully to model numerous fluid multilayer systems.[51-54] However, the experimental results, obtained in the current study, show that the layers of plastic rotator phase are thinner and stiffer than the initial estimate proposed in Refs. 1-2 which calls for reconsidering the assumptions made in the Evans' approach.

Considering the other extreme of bending a fully solid isotropic layer, the bending rigidity is proportional to h^3 according to Kirchhoff-Love theory of thin elastic shells,[54] rather

than proportional to h^2, as proposed by Evans[51] and adopted by us in Ref. 1. The assumption that K_B is proportional to h^3 leads to the following estimate:

$$h_{PL} \geq h_1(\gamma r^2/K_{B1})^{1/3} \quad (6)$$

where h_1 is monolayer thickness, γ is interfacial tension, r is curvature at the droplet edges, and K_{B1} is monolayer bending elasticity constant. Taking a high estimate, $K_{B1} \approx 10^{-17}$ J, as proposed by Guttmman et al.[17-19] and $h_1 \approx 2$ nm, yields minimum values for $h_{PL} \approx 16$ nm for $\gamma \approx 5$ mN/m and $h_{PL} \approx 7$ nm for $\gamma \approx 0.5$ mN/m. Lowest values of γ were measured with the surfactants from *Group A* which may explain why the respective drops could deform even with thin multilayers of rotator phase (2-3 layers only). Note that the assumption for drop shape transformation by a single monolayer requires a value of $K_{B1} \approx 10^{-16}$ J even for interfacial tension as low as $\gamma \approx 0.1$ mN/m – such a value of K_{B1} is an order of magnitude higher than the highest values reported or proposed in the literature.[17-19] Therefore, the only possibility for drop deformation by single adsorption monolayer is to have an oil-water interfacial tension which is of the order of 10^{-2} mN/m or lower.

We should note that it was difficult to predict which of these two models, expressed via eq. 5 or eq. 6, would predict better the behaviour of the plastic crystals without having experimental results like those obtained in the current study. We have used in our previous papers[1-3] the model by Evans & Skalak,[52] as the internal structure of the rotator phase resembles closer that of the bio-membranes, as compared to that of the isotropic solid shells. As explicitly stated by Evans "…bending theory for a three-dimensional isotropic material is clearly inappropriate to lipid bilayers".[51] The direct comparison of the predictions of these two models with the current experimental results for the thickness of the rotator phase in the deformed drops, allows us to conclude that the multilayers are strongly interlocked and have high shear resistance, closer to those in solid crystals. Hence, Kirchhoff-Love model[54] describes better these results, whereas Evans model[51] seems to overestimate the thickness of the rotator phase, despite being appropriate for describing the mechanical properties of fluid bio-membranes and their multilayers.

CONCLUSIONS

In the current article, we present systematic and complementary DSC measurements and optical observations of the drop self-shaping phenomenon. The obtained results show unambiguously that the drop-shape transformations observed upon cooling are caused by the formation of ordered multilayers of alkane molecules at the drop surface. The thickness of the

formed multilayer of rotator phase depends strongly on the type of surfactant used for emulsion stabilization and, to some extent, on the size and shape of the deformed drops:

For surfactants from *Group B* for which $T_d \approx T_m$ (where T_m is the melting temperature of the bulk alkane), the thickness of the rotator phase varies, depending on the initial drop diameter and the drop shape. For the polyhedrons and platelets, formed from 9.5 μm drops, this thickness is $h_{PL} \approx 55 \pm 15$ nm which corresponds to $\approx 24 \pm 6$ layers of molecules. For the elongated rods formed from smaller drops, 3 μm in diameter, the thickness of the rotator phase is estimated to be ≈ 10 nm, viz. around 4 ± 1 molecular layers.

The drop transformations in the presence of surfactants from *Group C* for which $T_d < T_m$, also induce measurable heat effects which, however, overlap partially with the freezing of a small fraction of the alkane drops. From the obtained results we could estimate the thickness of the rotator phase in these systems to be ≈ 8 nm, viz. around 3 ± 1 molecular layers.

For surfactants from *Group A* which induce drop shape deformations, starting at temperature $T_d > T_m$, we could not estimate the thickness of the ordered layer, because the result of this estimate depends very much on the assumptions made. By using different assumptions we found that the thickness of the ordered layer in these systems could vary between 5 and 180 nm, which correspond to between 2 and 80 molecular layers.

The results have also allowed us to determine whether the interlayer interactions in plastic crystals are closer to those in solid crystal structures or to those in bio-membranes (our original assumption in Ref. 1). Comparison of the model predictions to the obtained results allowed us to conclude that the measured thickness of the rotator phase is better described by the Kirchoff-Love theory of thin elastic shells[54] predicting $K_B \propto h_{PL}^3$, where K_B is the bending elastic modulus and h_{PL} is the thickness of the plastic rotator phase, formed on the drop surface. This information will be used to develop the thermodynamic model able to explain the self-shaping phenomenon.

The obtained results provide directions for optimization and rational control of the processes of drop self-shaping in the various systems and on the related process of drop bursting (self-emulsification) observed[7-8] in some of these emulsions.

Supporting information:

Supporting Information is available free of charge on the ACS Publications website.

Acknowledgements:

This work was funded by the European Research Council (ERC) grants to Stoyan Smoukov, EMATTER (# 280078) and Proof-of-Concept grant ShipShape (# 766656). The study falls under the umbrella of European networks COST MP 1305 and MP1106. ZV is grateful for the financial support provided for the execution of STSM project: Cost-STSM-MP1305-30666 and DC for the financial support for execution of STSM project: Cost-STSM-MP1106-071867, allowing them to become familiar with the DSC technique and to obtain important experimental results. The authors gratefully acknowledge the support from the Horizon 2020 project ID: 692146-H2020-eu.4.b "Materials Networking". Useful discussions with Dr. Ivan Lesov are gratefully acknowledged.

Figure captions - Supporting Information Video, Tables and Figures

Movie S1. Drop self-shaping observed upon cooling of 33 μm hexadecane drops, dispersed in 0.75 wt. % $C_{16}EO_{10}$ surfactant solution. The initial temperature in the sample is 23.9°C, the cooling is performed at a cooling rate 0.5°C/min. Some isolated drops start to deform at temperature around 23.5°C, but the main fraction of the drops start deforming around 22 ± 0.5°C. First complete freezing of a drop is observed at 15.4°C and most of the big drops freeze down to 14°C. The smaller drops, obtained in the process of drop breaking during cooling, freeze at slightly lower temperature.

Table S1. Properties of the alkanes studied.

Table S2. Properties and structural formulas of the surfactants used in the current study and in our previous[1,2] studies.

Table S3. Surfactant classification with respect to the temperature, T_d, at which the first drop shape deformations are observed (after Ref. 2).

Figure S1. Drop shape evolutionary scheme and mechanism of drop-shape transformations. (a) Drop-shape evolutionary scheme, showing the main stages through which the drops pass upon cooling. (b) Schematic presentation of the mechanism, causing drop shape transformations. A layer of plastic rotator phase of ordered alkane molecules is formed on the drop surface, in the areas where the surface acquires a cylindrical shape with a radius of curvature in the micrometer and sub-micrometer range. For more detailed information, see Refs. 1-6.

Figure S2. Experimental setup for optical observations in a glass capillary. (a) Schematic presentation of the cooling chamber, made of aluminium, with optical windows cut out, used for microscope observation of the emulsion samples. (b) The studied emulsions are contained in glass capillaries, placed in the thermostatic chamber and observed in transmitted light through the optical windows.

Figure S3. Experimental setup for optical observations in DSC pan. Two DSC pans, filled with emulsion samples, are placed in a thermostatic metal chamber. In the first pan, a thermo-couple probe is inserted in order to measure the temperature in the sample, while the sample in the second pan is observed with an optical microscope, in reflected white light, while performing cooling and heating of the emulsion.

Figure S4. Histograms of the drop size distributions measured for (a-b) $C_{16}/C_{16}SorbEO_{20}$ sample with d_{32} = 3 μm, (c-d) $C_{16}/C_{16}SorbEO_{20}$ sample with d_{32} = 9.5 μm and (e-f) $C_{16}/C_{16}EO_{20}$ sample with d_{32} = 2.6 μm. (a,c,e) Drop size distributions by number. (b,d,f) Drop size distributions by

volume. The dashed curves are fits to the experimental points by Gaussian distribution. For all samples the uncertainty in the calculation of the mean volume-surface diameter is ± 0.1 μm.

Figure S5. Microscopy pictures of C_{16} drops, stabilized by $C_{12}SorbEO_{20}$ surfactant. (a-c) Drop freezing upon cooling in glass capillary. The drops are observed in transmitted polarized light. (a) At temperature above 8ºC all drops are spherical and liquid. (b) At temperature around 7ºC some of the drops have frozen without any drop shape deformations seen. (c) All drops have frozen in a spherical shape at temperature around 5ºC. (d-e) Sample of the same emulsion placed in a DSC pan and observed in reflected light upon cooling. (d) From the very beginning of the observation, oil lenses are observed on the surface of the emulsion layer, due to coalescence of some of the oil droplets with the water-air interface. (e) At temperature around 15ºC, these oil lenses freeze, see the wrinkles on the surface of the frozen oils lens. Both experiments are performed at cooling rate 0.5°C/min. Scale bars, 50 μm.

Figure S6. Cooling thermograms of surfactant solutions. No measurable peaks are observed in the DSC measurements of 1.5 wt % $C_{16}EO_{20}$ (red curve), 0.75 wt % $C_{16}EO_{10}$ (blue curve) and 1.5 wt % $C_{16}SorbEO_{20}$ (green curve). These control experiments, performed at the same surfactant concentrations as with the respective emulsions, allow us to interpret the observed peaks in the emulsions thermograms as emerging entirely from ordering the alkane molecules inside the droplets. The heat flow is presented in 0.02 W/g range, similar to that used in Figure 7a,b from the main text and Supplementary information Figure S7, to illustrate the lack of any detectable signal in this scale. The small shift between the absolute values of the heat flow signal for the three surfactant solution sample is due to the small differences between the samples weight: $C_{16}EO_{20}$ 26.6 mg; $C_{16}EO_{10}$ 22.9 mg and $C_{16}SorbEO_{20}$ 22.4 mg. Presented thermograms are the one originally obtained from the measurement, no rescaling was done. Cooling rate in the experiments: 0.5°C/min.

Figure S7. Cooling thermogram of C_{12} drops, stabilized by $C_{16}EO_{20}$ surfactant. Although the emulsion is stabilized by surfactant with long hydrophobic chain length, the DSC thermogram does not show any measurable peaks in the temperature interval between 0 and 23°C. Thus, the peaks in the thermograms presented in the main text of the article are entirely due to the ordering of alkane molecules. The heat flow is presented in 0.02 W/g range, similar to that used in Figure 7a and b from the main text, to illustrate the lack of any detectable signal in this scale. The original signal obtained from the measurement is presented, no rescaling was done, cooling rate 0.5°C/min.

Figure S8. Heating thermograms of emulsions, heating rate 0.5 °C/min. For all samples, the heating peak is very sharp and observed in narrow temperature range. No other peaks are observed upon heating of the samples. (a) $C_{16}/C_{16}SorbEO_{20}$ emulsion with $d_{ini} \approx 3 \pm 0.1$ μm, the cooling thermogram of the same sample is presented as Figure 4 in the main text. (b) $C_{16}/C_{16}EO_{20}$ emulsion with $d_{ini} \approx 2.6 \pm 0.1$ μm, the cooling thermogram of the same sample is presented as Figure 6a in the main text. The vertical dashed lines are only guides to the eye. The thermograms are rescaled only with respect to the oil weight fraction, the baselines have not been shifted to "zero" value.

Figure S9. Cooling thermograms from the main article with reference lines showing the temperature interval over which the integration of the peak has been performed. All thermograms are obtained at cooling rate 0.5 °C/min. (a) $C_{16}/C_{16}SorbEO_{20}$ emulsion with $d_{ini} \approx 9.5 \pm 0.1$ μm, Figure 2 in the main text. The integration limit is set between the beginnings of the deformations (initial peak at high temperature) down to 12.2°C, where tetragonal platelets are formed. From this enthalpy we have estimated the thickness of the plastic rotator phase formed on the tetragonal platelets surface. (b) $C_{16}/C_{16}SorbEO_{20}$ emulsion with $d_{ini} \approx 3 \pm 0.1$ μm, Figure 4 from the main text. The integration limits are set between the beginnings of the curve deviation from its baseline value down to 13.8°C. From the obtained enthalpy we estimated the rotator phase thickness in the 15 μm rod-like particles. (c) $C_{16}/C_{16}EO_{20}$ emulsion with $d_{ini} \approx 2.6 \pm 0.1$ μm, Figure 6 from the main text. The integration limits are set between the beginnings of the curve deviation from its baseline value down to 6.5°C. Here, around 8% of the peaks enthalpy is due to the complete freezing of a fraction of the drops, while the rest of the enthalpy is due to rotator phase formation. From this enthalpy we estimated the thickness of the rotator phase formed on the surface of the long fibers, *Group C*. (d) $C_{16}/C_{16}EO_{10}$ emulsion with $d_{ini} \approx 33 \pm 0.4$ μm, Figures 7a,b from the main text. The integration limits are set between the beginnings of the curve deviation from its baseline value down to the end of the first distinct peak. Note that there is small deviation in the temperatures at which the peaks begin in the two graphs; therefore, the integration limits are slightly shifted in the two graphs, while keeping the width of the temperature interval fixed at 1.2°C. For more details about the experimental conditions see the main text.

Figure S10. Independently obtained cooling thermograms for the main emulsion systems presented in Figures 2, 4 and 6 of the main text. The blue dashed curves reproduce the curves presented in the main text. The percentage presents the oil weight fraction in the particular emulsion sample tested. (a-b) Cooling thermograms of C_{16} drops stabilized by $C_{16}SorbEO_{20}$

surfactant with initial drop diameter $d_{32} \approx 3$ μm: (a) two independently obtained cooling thermograms of two samples prepared from the same original emulsion; and (b) four cooling thermograms measured in experiments with four independently prepared original emulsions. (c) Three independently obtained cooling curves of C_{16} drops with initial diameter $d_{32} \approx 2.6$ μm, stabilized by $C_{16}EO_{20}$ surfactant. (d) Cooling thermograms of C_{16} drops with initial diameters $d_{32} \approx 9.5$ and $d_{32} \approx 13.3$ μm, stabilized by $C_{16}SorbEO_{20}$ surfactant. The normalized areas of the initial peaks used for determination of the rotator phase fraction are 3.8 % ± 0.6 % from the total enthalpy of drop freezing. For these emulsions, the bigger drops with $d_{32} \approx 13.3$ μm freeze a bit earlier in their evolution, because the statistical process of drop freezing has higher probability in the bigger drops [S1]. In all experiments, the cooling rate is 0.5°C/min.

Figure S11. (a) Sketch of the cutting required to connect the cylinders at the corners of the particle. (b) Calculation of the sides of the middle platelet.

Figure S12. (a) Sketch of the particle cross-section. The volume of the cylindrical frame is calculated as described in Section S1a, the volume of the middle platelet is calculated in Section S1b, and the volume of the connections – in Section S1c. (b) Geometry of the connections' cross-section.

Figure S13. (a) Sketch of the particle cross-section with rotator phase formed on the surface of the entire cylindrical frame. (b) Geometrical sketch of the model, used to calculate the rotator phase volume as defined in Model I. See text for more details.

Figure S14. Schematics of the two geometrical models, used to estimate the thickness of plastic rotator phase, located along the particle edges. (a) Model A: the cross-section of the rotator phase is assumed to be a circular segment. (b) Model B: the cross-section of the rotator phase is assumed to be a circular arc of homogeneous thickness. In both presentations, the volume filled with rotator phase is illustrated with light brown color. See text for more detailed explanations.

Figure captions

Figure 1. DSC thermogram and microscopy images for C_{16} drops with initial drop size, d_{ini} ≈ 10 μm, stabilized by $C_{16\text{-}18}EO_{50}$ surfactant (*Group D*). (a) DSC thermogram upon cooling; (b-d) Microscopy images in transmitted polarized light, showing the process of drop freezing upon cooling. The cooling experiment is performed in glass capillary. (b) The first freezing process is observed at temperature 9.3ºC, however as seen in this picture only a very small fraction of the drops has frozen down to 7.1ºC. (c-d) The main freezing process is observed between 6.5ºC and 5.6ºC. (e-f) Cooling experiment of the same sample, contained in a DSC pan. The drops are observed in reflected white light. The small peaks, observed in the thermogram around 15ºC are due to the freezing of the oil lenses and some large drops, formed after drop-drop coalescence. (e) Oil lenses are observed at the top of the sample, placed in a DSC pan. (f) Fluid big drop. (g) The drop freezes at a temperature 15.3ºC. All experiments (both DSC and optical observations) are performed at 0.5°C/min cooling rate. Scale bars, 20 μm.

Figure 2. DSC thermogram and microscopy images for C_{16} drops with d_{ini} ≈ 9.5 ± 0.1 μm, stabilized by $C_{16}SorbEO_{20}$ surfactant (*Group B*). (a) DSC thermogram, obtained at 0.5 °C/min cooling rate; (b-g) Microscopy pictures showing the different stages of the drop shape evolution upon cooling; cooling rate 0.5 °C/min. (b) All emulsion drops are spherical at temperatures above 17ºC. (c) Drop shape transformations start around 15.2 ± 0.2ºC (data from 4 independent measurements), for this particular sample the peak starts at 15.4ºC. At this temperature the DSC curve starts to deviate from the baseline. (d) At temperature around 14.2ºC flattened polyhedrons are formed. (e) The decrease of the temperature leads to further evolution in drop shape. At temperature around 12.2ºC, drops have evolved up to the stage of tetragonal platelets. (f) Some rare drops were observed to freeze at 11ºC ≤ T ≤ 12ºC, while most of the drops elongate into long fibers. (g) The thin elongated fibers freeze (crystallize) completely at T ≈ 6.5ºC. Scale bars, 10 μm.

Figure 3. Calculation of the rotator phase thickness for tetragonal platelets (*Group B*). (a) Microscopy image of fluid tetragonal platelets obtained upon cooling of C_{16} emulsion sample stabilized by $C_{16}SorbEO_{20}$ surfactant. The initial drop size is d_{ini} ≈ 9.5 μm, drops are cooled at 0.5 °C/min. Scale bar, 10 μm; (b) Sketch of a fluid platelet; (c-d) Sketches of two alternative models used to estimate the thickness of the rotator phase, formed at the platelet surface: (c) Model I: Geometrical model in which it is assumed that the rotator phase is formed only at the platelet periphery (in the regions of high interfacial curvature) while the alkane in the inner part of the drop is in a liquid state; (d) Model II: Geometrical model using the assumption that a homogeneous layer of rotator phase is formed over the entire surface of the deformed drop. See text for more details.

Figure 4. DSC thermogram and microscopy images for C_{16} drops, $d_{ini} \approx 3$ μm, stabilized by $C_{16}SorbEO_{20}$ surfactant (*Group B*). (a) DSC thermogram, obtained at 0.5 °C/min cooling rate; (b-g) Microscopy pictures showing the different stages of the drop shape evolution upon cooling; cooling rate 0.5 °C/min. (b) All emulsion drops are spherical at temperatures above 17.5ºC. (c) Significant drop shape transformations start in the range between 17 and 15 ºC. The initial weak deviation of the DSC curve from the baseline is followed by a sharp deviation at 15 ± 0.3 ºC (data from 10 independent measurements), for the thermogram presented on the figure, the curve deviates sharply at 14.7 ºC. (d) At temperature around 14.7ºC rod-shaped entities are formed. (e) At temperature around 13.5ºC the drops have evolved into long rods and first drop freezing is observed. (f) Thin fibers are formed around 12ºC, along with additional drop freezing. (g) All thin fibers freeze at temperature around 5.5ºC drops. Scale bars, 10 μm.

Figure 5. Calculation of the rotator phase thickness for the rod-like fluid drops (*Groups B and C*). Sketch of the geometrical model used for calculation of the rotator phase thickness in rod-like fluid drops. The rotator phase is formed with homogeneous thickness on the drop surface, while the core of the drop contains isotropic liquid (see text for details).

Figure 6. DSC thermogram and microscopy images for C_{16} drops, $d_{ini} \approx 2.6$ μm, stabilized by $C_{16}EO_{20}$ surfactant (*Group C*). (a) DSC thermogram, obtained at 0.5 °C/min cooling rate; (b-g) Microscopy pictures showing the different stages of the drop shape evolution upon cooling; cooling rate 0.5 °C/min. (b) All emulsion drops are spherical at temperatures above 11ºC. (c) Drop shape transformations start around 10.5ºC and drops rapidly evolve into short rods. At this temperature the DSC curve starts to deviate from the baseline. (d-e) With the decrease of the temperature, the rod length increases, while the diameter decreases. (f) Thin long fibers are formed from the rods. Some colored frozen drops are seen which had been frozen at higher temperatures, ca. at $T \approx 10$°C. (g) Freezing of the fibers. At this temperature the second peak in the DSC thermogram is observed. Scale bars, 10 μm.

Figure 7. DSC thermogram and microscopy images for C_{16} drops, $d_{ini} \approx 33$ μm, stabilized by $C_{16}EO_{10}$ surfactant (*Group A*). (a-b) DSC thermograms, obtained at 0.5 °C/min cooling rate from two independent measurements for the temperature interval between 16 and 26ºC. Note that although the peak observed between 20 and 22ºC is relatively small, it is well reproducible. Furthermore, the curve stays above the baseline value at $T < 22$ °C which reflects the continuous drop shape transformations in this temperature range. (c-d) Microscopy pictures showing the different stages of the drop shape evolution upon cooling; cooling rate 0.5 °C/min. (c) Most of the drops are spherical at temperatures above 22.5ºC, **see Movie S1**. (d) All of the drops have changed their shape at 21 ºC. The thermograms are rescaled only with respect to the oil weight fraction, the baselines have not been shifted to "zero" value.

References

1. Denkov, N.; Tcholakova, S.; Lesov, I.; Cholakova, D.; Smoukov, S. K. Self-shaping of oil droplets via the formation of intermediate rotator phases upon cooling. *Nature* **2015**, *528*, 392-395. doi: 10.1038/nature16189

2. Cholakova D.; Denkov N. D.; Tcholakova S.; Lesov I.; Smoukov S. K. Control of drop shape transformations in cooled emulsions. *Adv. Colloid Interface Sci.* **2016**, *235*, 90-107. doi: 10.1016/j.cis.2016.06.002

3. Denkov, N.; Cholakova, D.; Tcholakova, S.; Smoukov, S. K. On the mechanism of drop self-shaping in cooled emulsions. *Langmuir* **2016**, *32*, 7985-7991. doi: 10.1021/acs.langmuir.6b01626

4. Cholakova, D.; Valkova, Z.; Tcholakova, S.; Denkov, N.; Smoukov, S. K. "Self-shaping" of multicomponent drops. *Langmuir* **2017**, *33*, 5696-5706. doi: 10.1021/acs.langmuir.7b01153

5. Lesov, I.; Valkova, Z.; Vassileva, E.; Georgiev, G.; Ruseva, K.; Simeonov, M.; Tcholakova, S.; Denkov, N.; Smoukov, S. Bottom-up synthesis of polymeric micro- and nanoparticles with regular anisotropic shapes. *Macromolecules* **2018**, *51*, 7456-7462. doi: 10.1021/acs.macromol.8b00529

6. Gordon, R.; Hanczyc, M.; Denkov, N.; Tiffany, M.; Smoukov, S. K. Emergence of polygonal shapes in oil droplets and living cells: The potential role of tensegrity in the origin of life. In book: Habitability of the Universe before Earth. January **2018**, 427-490. doi: 10.1016/B978-0-12-811940-2.00018-6

7. Tcholakova, S.; Valkova, Z.; Cholakova, D.; Vinarov, Z.; Lesov, I.; Denkov, N.; Smoukov, S. K. Efficient self-emulsification via cooling-heating cycles. *Nat. Commun.* **2017**, *8*:15012. doi: 10.1038/ncomms15012

8. Valkova, Z.; Cholakova, D.; Tcholakova, S.; Denkov, N.; Smoukov, S. K. Mechanisms and control of self-emulsification upon freezing and melting of dispersed alkane drops. *Langmuir* **2017**, *33*, 12155-12170. doi: 10.1021/acs.langmuir.7b02048

9. Small, D. M. The Physical Chemistry of Lipids. From Alkanes to Phospholipids. *Plenum: New York*, **1986**.

10. Sirota, E.; King, H.; Singer, D.; Shao H. Rotator phases of the normal alkanes: An x-ray scattering study. *J. Chem. Phys.* **1993**, *98*, 5809-5824. doi: 10.1063/1.464874

11. Sirota, E.; Singer, D. Phase transitions among the rotator phases of the normal alkanes, *J. Chem. Phys.* **1994**, *101*, 10873-10882. doi: 10.1063/1.467837

12. Sirota, E.; Herhold, A. Transient phase-induced nucleation. *Science* **1999**, *283*, 529-532. doi: 10.1126/science.283.5401.529

13. Ueno, S.; Hamada, Y.; Sato, K. Controlling polymorphic crystallization of n-alkane crystals in emulsion droplets through interfacial heterogeneous nucleation. *Cryst. Growth Des.* **2003**, *3*, 935-939. doi: 10.1021/cg0300230

14. Shinohara, Y.; Takamizawa, T.; Ueno, S.; Sato, K.; Kobayashi, I.; Nakajima, M.; Amemiya, Y. Microbeam X-Ray diffraction analysis of interfacial heterogeneous nucleation in n-hexadecane inside oil-in-water emulsion droplets. *Cryst. Growth Des.* **2008**, *8*, 3123-3126. doi: 10.1021/cg701018x

15. Shinohara, Y.; Kawasaki, N.; Ueno, S.; Kobayashi, I.; Nakajima, M.; Amemiya Y. Observation of the transient rotator phase of n-hexadecane in emulsified droplets with time-resolved two-dimensional small- and wide-angle X-Ray scattering. *Phys. Rev. Lett*. **2005**, *94*, 097801-1 – 097801-4. doi: 10.1103/PhysRevLett.94.097801

16. Cholakova, D. Control of the shape of emulsion droplets undergoing phase transition, Bachelor's degree thesis, supervisor Prof. N. Denkov, reviewer Dr. K. Golemanov, **2016**, in Bulgarian.

17. Guttman, S.; Sapir, Z.; Schultz, M.; Butenko, A.; Ocko, B.; Deutsch, M.; Sloutskin, E. How faceted liquid droplets grow tails. *Proc. Natl. Acad. Sci. U.S.A.* **2016**, *113*, 493-496. doi: 10.1073/pnas.1515614113

18. Guttman, S.; Ocko, B.; Deutsch, M.; Sloutskin, E. From faceted vesicles to liquid icoshedra: Where topology and crystallography meet. *Curr. Opin. Colloid Interface Sci.* **2016**, *22*, 35-40. doi: 10.1016/j.cocis.2016.02.002

19. Guttman, S.; Sapir, Z.; Ocko, B.; Deutsch, M.; Sloutskin, E. Temperature-tuned faceting and shape changes in liquid alkane droplets. *Langmuir*, **2017**, *33*, 1305-1314. doi: 10.1021/acs.langmuir.6b02926

20. Höhne, G.; Hemminger, W.; Flammersheim, H. Differential scanning calorimetry. *Springer*, **2003**. doi: 10.1007/978-3-662-06710-9.

21. Gunther, E.; Hiebler, S.; Mehling, H.; Redlich, R. Enthalpy of phase change materials as a function of temperature required accuracy and suitable measurement methods. *Int J Thermophys*. **2009**, *30*, 1257-1269. doi: 10.1007/s10765-009-0641-z

22. Gill, P.; Moghadam, T.; Ranjbar, B. Differential scanning calorimetry techniques: applications in biology and nanoscience. *J Biomol Tech.* **2010**, *21*, 167-193. pmcid: pmc2977967
23. Clas, S.-D.; Dalton, C.; Hancock, B. Differential scanning calorimetry: applications in drug development. *Pharm. Sci. Technol. Today*. **1999**, *2*, 311-320. doi: 10.1016/S1461-5347(99)00181-9.
24. Bruylants, G.; Wouters, J.; Michaux, C. Differential scanning calorimetry in life science: Thermodynamics, stability molecular recognition and application in drug design. *Curr. Med. Chem.* **2005**, *12*, 2011-2020. doi: 10.2174/0929867054546564
25. Spink, C. Differential scanning calorimetry. *Methods Cell Bio.* **2008**, *84*, 115-141. doi: 10.1016/S0091-679X(07)84005-2
26. Biliaderis, C. Differential scanning calorimetry in food research – A review. *Food Chem.* **1983**, *10*, 239-265. doi: 10.1016/0308-8146(83)90081-X
27. Slade, L.; Levine, H. Glass transitions and water-food structure interactions. *Adv. Food Nutr. Res.* **1995**, *38*, 103-269. doi: 10.1016/S1043-4526(08)60084-4
28. Nishinari, K. Rheological and DSC study of sol-gel transition in aqueous dispersions of industrially important polymers and colloids. *Colloid Polym. Sci.* **1997**, *275*, 1093. doi:10.1007/s003960050189
29. Johnson, C. Differential scanning calorimetry as a tool for protein folding and stability. *Arch. Biochem. Biophys.* **2013**, *531*, 100-109. doi: 10.1016/j.abb.2012.09.008
30. Demetzos, C. Differential scanning calorimetry (DSC): A tool to study the thermal behavior of lipid bilayers and liposomal stability. *J. Liposome Res.* **2008**, *18*, 159-173. doi: 10.1080/08982100802310261
31. Velez, C.; Khayet, M.; Ortiz de Zarate, J. M. Temperature-dependent thermal properties of solid/liquid phase change even-numbered n-alkanes: n-hexadecane, n-octadecane and n-eicosane. *Appl. Energy* **2015**, *143*, 383-394. doi: 10.1016/j.apenergy.2015.01.054
32. Knothe, G.; Dunn, R. A comprehensive evaluation of the melting points of fatty acids and esters determined by differential scanning calorimetry. *J. Am. Oil Chem. Soc.* **2009**, *86*, 843-856. doi:10.1007/s11746-009-1423-2
33. Clausse, D. Differential thermal analysis, differential scanning calorimetry, and emulsions. *J. Therm. Anal. Calorim.* **2010**, *101*, 1071-1077. doi: 10.1007/s10973-010-0712-1

34. Clausse, D.; Gomez, F.; Pezron, I.; Komunjer, L.; Dalmazzone, C. Morphology characterization of emulsions by differential scanning calorimetry. *Adv. Colloid Interface Sci.* **2005**, *117*, 59-74. doi: 10.1016/j.cis.2005.06.003
35. Dalmazzone, C.; Noik, C.; Clausse, D. Application of DSC for emulsified system characterization. *Oil Gas Sci. Technol. – Rev. IFP* **2009**, *5*, 543-555. doi: 10.2516/ogst:2008041
36. Potier, L.; Raynal, S.; Seiller, M.; Grossiord, J-L.; Clausse, D. Study of state transitions within multiple w/o/w emulsions using calorimetry (DSC). *Thermochim. Acta* **1992**, *204*, 145-155. doi: 10.1016/0040-6031(92)80323-O
37. Palanuwech, J.; Coupland, J. Effect of surfactant type on the stability of oil-in-water emulsions to dispersed phase crystallization. *Colloid Surf. A* **2003**, *223*, 251-262. doi:10.1016/S0927-7757(03)00169-9
38. Gülseren, I.; Coupland, J. Excess ultrasonic attenuation due to solid-solid and solid-liquid transitions in emulsified octadecane. *Cryst. Growth Des.* **2007**, *7*, 912-918. doi: 10.1021/cg060683f
39. McClements, D. J.; Dungan, S.; German, J.; Simoneau, C.; Kinsella, J. Droplet size and emulsifier type affect crystallization and melting of hydrocarbon-in-water emulsions. *J.Food Sci.* **1993**, *58*, 1148-1178. doi: 10.1111/j.1365-2621.1993.tb06135.x
40. Gülseren, I.; Coupland, J. Surface melting in alkane emulsion droplets as affected by surfactant type. *J. Am. Oil Chem. Soc.* **2008**, *85*, 413-419. doi: 10.1007/s11746-008-1216-z
41. Xie, B.; Liu, G.; Jiang, S.; Zhao, Y.; Wang, D. Crystallization behaviors of *n*-octadecane in confined space: Crossover of rotator phase from transient to metastable induced by surface freezing. *J. Phys. Chem. B*, **2008**, *112*, 13310-13315. doi: 10.1021/jp712160k
42. Kandori, K.; Gaonkar, A. (Ed.). Applications of microporous glass membranes: membrane emulsification. *Elsevier* **1995**, *Chapter 7*, 113-142. doi: 10.1016/B978-044481500-2/50009-8
43. Charcosset, C.; Limayem, I.; Fessi, H. The membrane emulsification process – a review. *J. Chem. Technol. Biotechnol.* **2004**, *79*, 209-218. doi: 10.1016/S0927-7757(02)00167-X
44. Christov, N.; Ganchev, D.; Vassileva, N.; Denkov, N.; Danov, K.; Kralchevsky, P. Capillary mechanisms in membrane emulsification: oil-in-water emulsions stabilized by Tween 20 and milk proteins. *Colloids Surf. A* **2002**, *209*, 83-104. doi: 10.1016/S0927-7757(02)00167-X

45. Nakashima, T.; Shimizu, M.; Kukizaki, M. Membrane emulsification by microporous glass. *Key Eng. Mater.* **1992**, *61-62*, 513-516. doi: 10.4028/www.scientific.net/KEM.61-62.513

46. Svarovsky, L. Solid-Liquid Separation 4th edn, Butterworth-Heinemann, **2000**.

47. Newton, R. H.; Haffegee, J. P.; Ho, M. H. Polarized light microscopy of weakly birefringent biological specimens. *J. Microsc.* **1995**, *180*, 127-130. doi: 10.1111/j.1365-2818.1995.tb03667.x

48. Holmberg, K. Handbook of applied surface and colloid chemistry. Vol. 2 Ch. 16 Identification of lyotropic liquid crystalline mesophases. *John Wiley & Sons* **2001**, 299-332. ISBN: 978-0-471-49083-8

49. Tokiwa, Y.; Sakamoto, H.; Takiue T.; Aratono, M.; Matsubara H.; Bain, C. Effect of surface freezing on stability of oil-in-water emulsions. *Langmuir*. **2018**, *34*, 6205-6209. doi: 10.1021/acs.langmuir.8b01088

50. Mondieig, D.; Rajabalee, F.; Metivaud, V. n-Alkane Binary Molecular Alloys. *Chem. Mater.* **2004**, *16*, 786-798. doi: 10.1021/cm031169p

51. Evans, E.A. Bending Resistance and Chemically Induced Moments in Membrane Bilayers, *Biophysical J.* **1974**, *14*, 923-931. doi: 10.1016/S0006-3495(74)85959-X

52. Evans, E.; Skalak, R. *Mechanics and thermodynamics of biomembranes*. *CRC*, **1980**.

53. Bermúdez, H.; Hammer, D. A.; Discher D. E. Effect of Bilayer Thickness on Membrane Bending Rigidity. *Langmuir* **2004**, *20*, 540-543. doi: 10.1021/la035497f

54. Love, A.E.H. The small free vibrations and deformation of a thin elastic shell, *Philosophical Transactions of the Royal Society A: Mathematical, physical and engineering sciences*; Published on 1 January **1888**. doi: 10.1098/rsta.1888.0016.

Table of Contents graphic